

# Global Biogeochemical Cycles

## RESEARCH ARTICLE

10.1029/2018GB005973

### Key Points:

- We implemented plant-mycorrhizal symbioses into a global terrestrial carbon-nitrogen cycle model
- The model reproduced contrasting responses from two elevated CO<sub>2</sub> experiments with different mycorrhizal associations
- In global simulations, changes in symbiotic nitrogen uptake pathways over time facilitated additional carbon storage under elevated CO<sub>2</sub>

### Supporting Information:

- Supporting Information S1

### Correspondence to:

B. N. Sulman,  
sulmanbn@ornl.gov

### Citation:

Sulman, B. N., Shevliakova, E., Brzostek, E. R., Kivlin, S. N., Malyshev, S., Menge, D. N. L., & Zhang, X. (2019). Diverse mycorrhizal associations enhance terrestrial C storage in a global model. *Global Biogeochemical Cycles*, 33, 501–523. <https://doi.org/10.1029/2018GB005973>






Received 2 MAY 2018

Accepted 20 MAR 2019

Accepted article online 23 MAR 2019

Published online 17 APR 2019

## Diverse Mycorrhizal Associations Enhance Terrestrial C Storage in a Global Model

Benjamin N. Sulman<sup>1,2,3</sup> , Elena Shevliakova<sup>4</sup>, Edward R. Brzostek<sup>5</sup> , Stephanie N. Kivlin<sup>6</sup>, Sergey Malyshev<sup>4,7</sup> , Duncan N.L. Menge<sup>8</sup> , and Xin Zhang<sup>9,10</sup> 

<sup>1</sup>Program in Atmospheric and Oceanic Sciences, Department of Geosciences, Princeton University, Princeton, NJ, USA, <sup>2</sup>Sierra Nevada Research Institute, University of California, Merced, Merced, CA, USA, <sup>3</sup>Environmental Sciences Division and Climate Change Science Institute, Oak Ridge National Laboratory, Oak Ridge, TN, USA, <sup>4</sup>NOAA Geophysical Fluid Dynamics Laboratory, Princeton, NJ, USA, <sup>5</sup>Department of Biology, West Virginia University, Morgantown, WV, USA, <sup>6</sup>Department of Ecology and Evolutionary Biology, University of Tennessee, Knoxville, TN, USA, <sup>7</sup>Department of Ecology and Evolutionary Biology, Princeton University, Princeton, NJ, USA, <sup>8</sup>Department of Ecology, Evolution, and Environmental Biology, Columbia University, New York, NY, USA, <sup>9</sup>Woodrow Wilson School of Public and International Affairs, Princeton University, Princeton, NJ, USA, <sup>10</sup>University of Maryland Center for Environmental Science, Frostburg, MD, USA

**Abstract** Accurate projections of the terrestrial carbon (C) sink are critical to understanding the future global C cycle and setting CO<sub>2</sub> emission reduction goals. Current earth system models (ESMs) and dynamic global vegetation models (DGVMs) with coupled carbon-nitrogen cycles project that future terrestrial C sequestration will be limited by nitrogen (N) availability, but the magnitude of N limitation remains a critical uncertainty. Plants use multiple symbiotic nutrient acquisition strategies to mitigate N limitation, but current DGVMs omit these mechanisms. Fully coupling N-acquiring plant-microbe symbioses to soil organic matter (SOM) cycling within a DGVM for the first time, we show that increases in N acquisition via SOM decomposition and atmospheric N<sub>2</sub> fixation could support long-term enhancement of terrestrial C sequestration at global scales under elevated CO<sub>2</sub>. The model reproduced elevated CO<sub>2</sub> responses from two experiments (Duke and Oak Ridge) representing contrasting N acquisition strategies. N release from enhanced SOM decomposition supported vegetation growth at Duke, while inorganic N depletion limited growth at Oak Ridge. Global simulations reproduced spatial patterns of N-acquiring symbioses from a novel niche-based map of mycorrhizal fungi. Under a 100-ppm increase in CO<sub>2</sub> concentrations, shifts in N acquisition pathways facilitated 200 Pg C of terrestrial C sequestration over 100 years compared to 50 Pg C for a scenario with static N acquisition pathways. Our results suggest that N acquisition strategies are important determinants of terrestrial C sequestration potential under elevated CO<sub>2</sub> and that nitrogen-enabled DGVMs that omit symbiotic N acquisition may underestimate future terrestrial C uptake.

**Plain Language Summary** Plants grow faster when there is more carbon dioxide (CO<sub>2</sub>) in the air. Because plant growth removes CO<sub>2</sub> from the air, this faster plant growth could lessen the warming that is caused by CO<sub>2</sub> emissions from human activities. However, plants also need nitrogen to grow, and the availability of this nutrient could constrain, or “limit,” how much CO<sub>2</sub> plants can remove from the air. Correctly predicting the degree of nitrogen limitation of plant growth is a major challenge for global land models. Some plants can overcome nitrogen limitation by partnering with fungi that extract nitrogen from the soil or with bacteria that extract nitrogen from the air. We incorporated these plant-microbe partnerships into a global land model, and we show that these partnerships could sustain plant growth under rising CO<sub>2</sub> concentrations. This suggests that existing models and experiments that do not include these partnerships may underestimate the potential for future CO<sub>2</sub> uptake by plants.

## 1. Introduction

Terrestrial ecosystems absorb as much as 29% of anthropogenic carbon dioxide (CO<sub>2</sub>) emissions, and the persistence of the terrestrial carbon (C) sink is a critical component of coupled climate-carbon cycle projections (Ciais et al., 2013; Le Quere et al., 2018). Rising atmospheric CO<sub>2</sub> concentrations can accelerate photosynthesis, increasing the rate of CO<sub>2</sub> removal from the atmosphere. While some observational evidence suggests that the terrestrial C sink is accelerating due to this stimulatory effect (Campbell et al.,

2017; Cole et al., 2009; Keenan et al., 2016), the magnitude and persistence of this enhancement of productivity remain uncertain (Beedlow et al., 2004; Körner, 2006).

One major source of uncertainty is the role of N availability, which could limit terrestrial C sequestration (Ciais et al., 2013; Wieder et al., 2015; Zhang et al., 2014). Limitation of plant C accumulation by N availability has been supported by stoichiometric arguments (Hungate et al., 2003; Zaehle, Friedlingstein, et al., 2010), global model simulations (e.g., Wieder et al., 2015), and ecosystem-scale observations (Norby et al., 2010). Plant N uptake in these models is typically limited by the release of inorganic or low molecular weight organic N compounds via decomposition of organic matter pools in the soil or litter (e.g., Gerber et al., 2010; Thomas et al., 2015; Zaehle, Friend, et al., 2010). These views of N limitation treat plant N acquisition as a source-limited process. While the production of bioavailable N via decomposition processes in these models is controlled by the N content of decomposing organic matter pools, the turnover rates of these pools are generally assumed to be inherent properties of the pools and independent of plant nutrient demands. Likewise, these models often assume inflexible responses of vegetation to N limitation, with plants restricting primary production when there is insufficient N to build new tissues (e.g., Gerber et al., 2010; Thomas et al., 2015; Thornton et al., 2007), although Gerber et al. (2010) did include dynamic responses of symbiotic N fixation to plant N limitation and Shi et al. (2016) integrated a model of dynamic N acquisition costs and strategies into the Community Land Model.

A developing understanding of soil organic matter (SOM) cycling has begun to highlight the critical role of microbial processes and plant-microbial interactions in driving the turnover of SOM pools and the associated production of plant-available N (Schmidt et al., 2011). Related advances in both modeling and conceptual understanding have challenged the paradigm underlying previous assessments by showing that plants are not passive recipients of soil N released by decomposition, but instead are active drivers of soil N cycling (Cheng et al., 2014; Drake et al., 2011; Lambers et al., 2008). Deposition of root cells, mucilage, and organic compounds to the rhizosphere can shape microbial communities and prime microbial cycling of C and N (Cheng et al., 2014; Phillips et al., 2012; Yuan et al., 2018). The deposition rate of these substrates to the rhizosphere has been shown to respond to plant N limitation (Phillips et al., 2009), and rhizosphere microbial responses can influence soil C and N cycling at ecosystem scales (Cheng et al., 2014; Finzi et al., 2015; Sulman et al., 2017). In addition, most land plants can acquire N through symbiotic relationships that can be broadly categorized into three mechanisms: Arbuscular mycorrhizal (AM) fungi primarily scavenge inorganic N from soil solution, effectively expanding the volume of soil that roots can access (George et al., 1995). Ectomycorrhizal (ECM) and ericoid fungi can play more active roles in SOM decomposition by producing extracellular enzymes to extract N from complex organic compounds in the soil and litter (Read & Perez Moreno, 2003), although these groups contain broad distributions of species and lineages with varying decomposition capabilities (Pellitier & Zak, 2017). Finally, N<sub>2</sub> fixing bacteria acquire N from atmospheric N<sub>2</sub> gas (Huss-Danell, 1997; Sprent, 2009).

Ecosystem-scale field experiments have suggested that acceleration of the soil N cycle by plant-microbe symbioses can facilitate continued plant growth under elevated CO<sub>2</sub> (Drake et al., 2011). Likewise, syntheses have indicated that mycorrhizal N uptake is an important contributor to ecosystem productivity under global change at large scales (Kivlin et al., 2013; Terrer et al., 2016, 2017) and model simulations have highlighted the potential for symbiotic N acquisition to at least partially ameliorate N limitation (Baskaran et al., 2016; Orwin et al., 2011; Sulman et al., 2017), suggesting that past assessments may have underestimated the potential for these mechanisms to enhance N uptake under elevated CO<sub>2</sub>. However, the effectiveness, persistence, and geographical distributions of these mechanisms remain under debate (Norby et al., 2017) and their potential impacts have not been quantified at global scales. One key uncertainty is the long-term efficacy of priming effects for supporting continued acceleration of plant N acquisition: Are they transient responses, or can they support long-term growth? Past and current elevated CO<sub>2</sub> experiments, which operate on a decadal time-scale, may not have had treatment durations lasting long enough to resolve long-term depletion of soil N pools mobilized by priming effects (Norby & Zak, 2011). In the absence of direct observations, mechanistic models that include key soil processes such as trapping of N-rich microbial-derived organic matter in stable mineral-organic associations (Bingham & Cotrufo, 2016) and depletion of soil C stocks associated with microbial mining of N from SOM (Sulman et al., 2017) can be used to estimate potential long-term impacts of elevated CO<sub>2</sub> levels. A second key uncertainty is the lack of observational

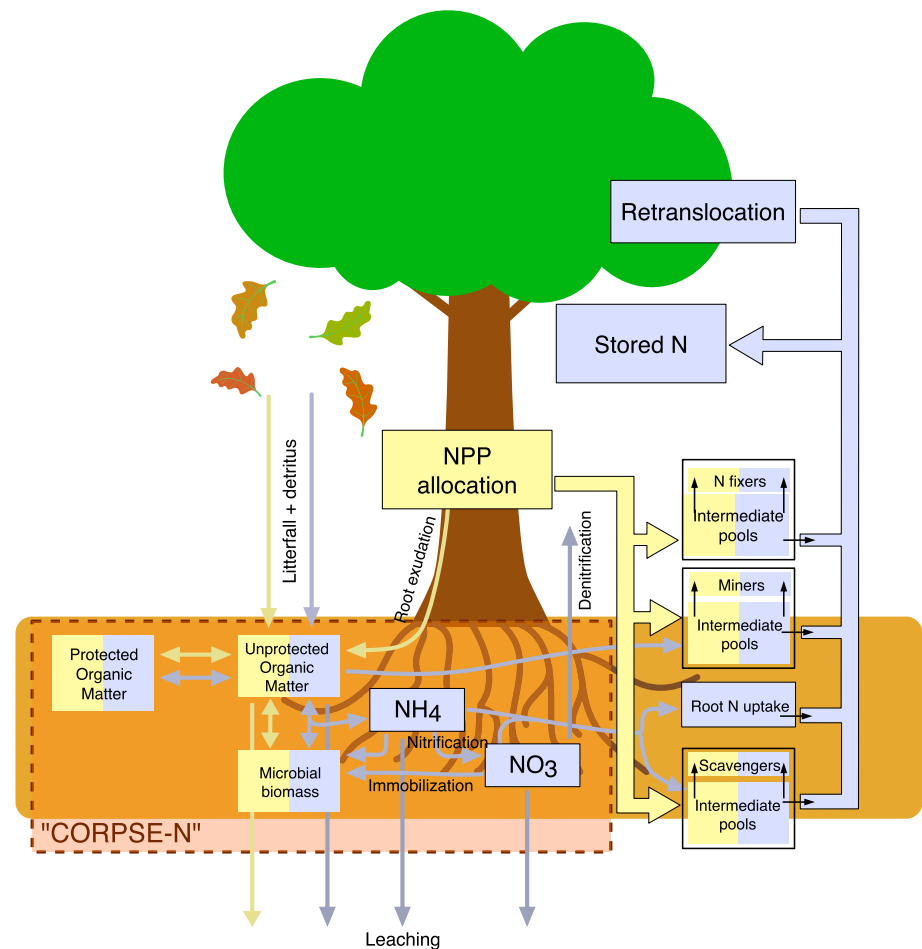


**Figure 1.** Diagram of C and N flows in the model. Yellow shows C stocks and flows, and purple shows N stocks and flows.

maps of mycorrhizal associations connected with these N acquisition strategies, which limits our ability to predict where plants have the capacity to access organic versus inorganic pools of N.

Given the critical role of terrestrial C sink projections in understanding climatic changes and informing potential policy responses, it is imperative for DGVMs and ESMs to incorporate these recent advances in our understanding of terrestrial N cycling. To meet this challenge, we implemented a new coupled plant-microbe-soil C-N cycling framework, Symbiotic Nitrogen Acquisition by Plants (SNAP; Figure 1) within the Geophysical Fluid Dynamics Laboratory (GFDL) land model LM3 (Milly et al., 2014). LM3-SNAP simulates plant N acquisition via the symbiotic inorganic N scavenging, SOM decomposition, and N<sub>2</sub> fixation mechanisms described above. Plant C is allocated among these mechanisms by calculating the return on investment (ROI): the amount of N returned to the plant by a symbiosis divided by the amount of plant C allocated to that symbiosis, following Brzostek et al. (2014) and Terrer et al. (2017). In addition, LM3-SNAP simulates N losses to waterways through leaching and to the atmosphere via denitrification. By coupling the vegetation and hydrology components of the land surface model to a state-of-the-art SOM model with explicit representation of microbial decomposition and physicochemical protection of SOM (Sulman et al., 2014, 2017), LM3-SNAP simulates interactions among N acquisition strategies, plant N uptake, N losses, and SOM cycling. We conducted simulations of two well-studied ecosystem-scale free air carbon enrichment (FACE) experiments (Duke and Oak Ridge National Laboratory) (1) to evaluate the model in the context of observations and investigate contrasts in ecosystem responses to elevated CO<sub>2</sub> among AM- and ECM-dominated ecosystems. We then conducted global-scale simulations and developed a novel, empirical global-scale map of ECM and AM fungal distributions (2) to evaluate how patterns of nitrogen availability and demand determine global patterns of plant N acquisition. Finally, we simulated a global-

scale elevated CO<sub>2</sub> manipulation (3) to project how contrasting assumptions about potential shifts in N acquisition strategies could affect projected changes in terrestrial C storage under elevated CO<sub>2</sub>.

## 2. Methods

Simulations used a modified version of the GFDL land model LM3, which forms the dynamic land component of the GFDL ESM 2.1. LM3 simulates C cycling in vegetation and soil (Shevliakova et al., 2009) as well as water and energy fluxes through vegetation, soils, and canopy air space (Milly et al., 2014). We augmented the previous soil and vegetation C cycle components of LM3 with the SNAP model, a new coupled C-N cycle framework combining the C-N version of the Carbon Organisms Rhizosphere and Protection in the Soil Environment (CORPSE-N) model (Sulman et al., 2017) with an explicit model of plant-microbial symbioses (Figure 1). We summarize the primary features of the model here and provide details and equations below. See Table S2 in the supporting information for a full list of parameter values, units, and sources. Model parameter values were determined using observed or literature values when possible and by fitting to observed patterns of carbon and nitrogen cycling when literature values were not available or parameters were not well matched to measured quantities. Some parameters, particularly those controlling symbiont growth and nitrogen acquisition rates, were not well constrained by available data.

The SOM decomposition component of the model explicitly represents microbial decomposition of organic matter and divides SOM into protected and unprotected components to represent physicochemical stabilization. Unprotected SOM is converted into protected SOM at a first-order rate that varies with soil clay content, with microbe-derived organic matter becoming protected at the fastest rate. Protected SOM is transferred back to the unprotected state using a fixed first-order rate. Only the unprotected fraction of SOM is accessible to microbial decomposition. In addition to free-living soil microbes, N-mining mycorrhizae can decompose unprotected SOM. Plant roots and N-scavenging mycorrhizae take up inorganic N released by decomposition.

Plant C allocation to symbioses (as a fraction of NPP) increases as plants deplete stored N reserves and become more N limited. This C allocation is partitioned among symbioses based on the relative ROI for each symbiosis, following Brzostek et al. (2014). The dynamic partitioning of C among strategies allows the model to respond to changing conditions of soil organic N pools and decomposition rates, symbiotic microbial biomass, and N availability, allowing for emergent ecosystem responses to N limitation. For example, when there is abundant inorganic N, scavenging by AM fungi is the most effective strategy and receives the greatest fraction of allocated C. As AM biomass grows, the saturating nature of its N uptake response combined with depletion of soil inorganic N reduces its marginal benefit and other strategies become comparatively more effective. When inorganic N is limited, N mining by ECM fungi receives a greater allocation fraction. When plant N demand outstrips the ability of both mycorrhizal types to extract N from the soil, symbiotic N<sub>2</sub> fixation becomes a more beneficial strategy despite its higher cost.

### 2.1. Model Details and Equations

#### 2.1.1. Plant N Use and C Allocation to Symbioses

While plant C cycling in the model generally followed previous LM3 functionality (Milly et al., 2014; Shevliakova et al., 2009), we added a N cycle component to plant growth and tissues in order to simulate N demand and related growth limitations. N taken up by plants was transferred to a stored N pool, which was used to produce vegetation biomass. Each tissue (leaves, roots, sapwood, and heartwood) had a fixed C:N ratio that varied by plant functional type (e.g., grassland, evergreen forest, and deciduous forest). In simulations with N-limited plant growth, if there was not enough N in the storage pool to support biomass growth, then biomass was limited to available N and excess plant C was left in the nonstructural carbohydrate pool.

After calculating the distribution of C and N in vegetation tissues, the remaining stored N was used to calculate plant N stress, which increased as stored N was depleted. N stress was calculated by comparing the stored N pool to a target value equivalent to double the leaf and root N content, based on the role of N storage in regrowth following herbivory (Millard et al., 2001):

$$N_{\text{stress}} = \frac{2(N_{\text{leaf}} + N_{\text{root}}) - N_{\text{storage}}}{N_{\text{leaf}} + N_{\text{root}}} \quad (1)$$

where  $N_{\text{leaf}}$ ,  $N_{\text{root}}$ , and  $N_{\text{storage}}$  are the N contents of leaves, fine roots, and the storage pool, respectively. Note that since the minimum  $N_{\text{storage}}$  was zero,  $N_{\text{stress}}$  had a maximum value of 2. This calculation ignored phenology (using growing-season leaf and root biomass allometry throughout the year), so that  $N_{\text{stress}}$  could be calculated during the winter in deciduous ecosystems.

$N_{\text{stress}}$  was used to calculate the amount of C allocated to N acquisition, with allocation rising as the stress level increased (except in simulations with no N limitation, which ignored changes in N stress):

$$C_{\text{transfer}} = \max(NPP, 0) f_{\text{Nalloc}} N_{\text{stress}} \quad (2)$$

where  $f_{\text{Nalloc}}$  is a parameter controlling allocation fraction. Dynamic allocation of a fraction of NPP to root exudation allowed the model to respond to changing conditions of N availability and plant growth rates. As plants depleted their N stores relative to their needs for building leaf and root biomass, a greater fraction of NPP was diverted to N acquisition, decreasing plant biomass accumulation but potentially mitigating N limitation of growth.

C allocated to N acquisition was partitioned among symbioses based on the relative ROI for each symbiosis, following the C cost optimization structure of Brzostek et al. (2014). However, while Brzostek et al. (2014) calculated C costs of N acquisition using cost functions specific to each N acquisition strategy, in our model C costs and ROI were determined dynamically by calculating plant N acquisition ( $N_j$ ) per unit of symbiont biomass ( $B_j$ ) multiplied by efficiency of symbiont biomass production ( $\epsilon_j$ ) and turnover time for that symbiont ( $\tau_j$ ). This metric incorporated the individual dynamics of each strategy as well as the efficiency of C allocation to that strategy.

$$ROI_j = \frac{N_j \tau_j \epsilon_j}{B_j} \quad (3)$$

where  $ROI_j$  is return on investment for strategy  $j$ . ROI for root exudation to the rhizosphere was calculated using the ratio of root N uptake to root biomass. C allocation was partitioned proportionally to each symbiosis based on ROI:

$$f_{\text{alloc},j} = \frac{ROI_j}{\sum_j ROI_j} \quad (4)$$

where  $f_{\text{alloc},j}$  is the fraction allocated to strategy  $j$ .

Detritus from leaf senescence, root turnover, and wood loss was transferred to litter and soil pools. A fixed fraction of C and N was retranslocated from leaves and roots during annual senescence and transferred back into the nonstructural carbohydrate and stored N pools.

### 2.1.2. Soil C and N Cycling

Soil C and N cycling were simulated using the C-N version of the CORPSE-N model (Figure 1; Sulman et al., 2017). Organic matter (OM) was divided into three classes, representing labile, chemically complex, and microbial necromass compounds. To represent physical protection processes such as aggregation and sorption to mineral surfaces, each class of OM was divided into protected and unprotected fractions. Unprotected OM was subject to microbial decomposition, transfers via litter inputs or leaching, and transformation between unprotected and protected states:

$$\frac{dC_{U,i}}{dt} = I_{C,i} - L_{C,i} - D_{C,i} - D_{C,i,\text{denit}} + \frac{\max(C_M - C_{M,\text{min}} * \sum_i C_{U,i}, 0)}{\tau_{\text{mic}}} f_{t,i} \epsilon_t - \frac{dC_{P,i}}{dt} \quad (5)$$

$$\frac{dN_{U,i}}{dt} = I_{N,i} - L_{N,i} - D_{N,i} - D_{N,i,\text{denit}} + \frac{1}{C:N_m} \frac{\max(C_M - C_{M,\text{min}} * \sum_i C_{U,i}, 0)}{\tau_{\text{mic}}} f_{t,i} \epsilon_t - \frac{dN_{P,i}}{dt} \quad (6)$$

where  $C_{U,i}$  and  $N_{U,i}$  are unprotected C and N, respectively;  $I_{C,i}$  and  $I_{N,i}$  are external inputs of C and N such as litter deposition and root exudation;  $D_{C,i}$  and  $D_{N,i}$  are aerobic decomposition rates of C and N, respectively;

$D_{C,i,denit}$  and  $D_{N,i,denit}$  are anaerobic decomposition rates supported by denitrification;  $\frac{\max(C_M - C_{M,min} * \sum_i C_{U,i}, 0)}{\tau_{mic}}$ ,  $f_{t,i} \epsilon_t$  and  $\frac{1}{C:N_m} \frac{\max(C_M - C_{M,min} * \sum_i C_{U,i}, 0)}{\tau_{mic}}$  are deposits of microbial necromass (see equations (12) and (13));  $L_{C,i}$  and  $L_{N,i}$  are net leaching losses of dissolved C and N; and  $\frac{dC_{P,i}}{dt}$  and  $\frac{dN_{P,i}}{dt}$  are net transfers of C and N to or from the protected state. The  $i$  subscript refers to the three chemically defined OM classes.

Protected C and N were formed from unprotected organic matter and converted back to unprotected form at first-order rates:

$$\frac{dC_{P,i}}{dt} = C_{U,i} \cdot \gamma_i - \frac{C_{P,i}}{\tau_P} \quad (7)$$

$$\frac{dN_{P,i}}{dt} = N_{U,i} \cdot \gamma_i - \frac{N_{P,i}}{\tau_P} \quad (8)$$

where  $\gamma_i$  is the protection rate for each OM type and  $\tau_P$  is the turnover time of protected OM. The decomposition rate of unprotected OM was controlled by microbial biomass ( $C_M$ ), temperature ( $T$ ), and volumetric soil water content ( $\theta$ ). C and N components of unprotected OM were decomposed at proportional rates:

$$D_{C,i} = V_{max,i}(T) \cdot \left(\frac{\theta}{\theta_{sat}}\right)^3 \left(1 - \frac{\theta}{\theta_{sat}}\right)^{2.5} \frac{1}{f_{\theta,max}} \cdot C_{U,i} \frac{C_M/C_{U,i}}{C_M/C_{U,i} + k_M} \quad (9)$$

$$D_{N,i} = V_{max,i}(T) \cdot \left(\frac{\theta}{\theta_{sat}}\right)^3 \left(1 - \frac{\theta}{\theta_{sat}}\right)^{2.5} \frac{1}{f_{\theta,max}} \cdot N_{U,i} \frac{C_M/C_{U,i}}{C_M/C_{U,i} + k_M} \quad (10)$$

where  $\theta_{sat}$  is the saturation level of  $\theta$  and  $\frac{1}{f_{\theta,max}}$  is a factor normalizing the  $\theta$  dependence to a maximum value of one. Note that the decomposition rate was controlled by the ratio of microbial biomass carbon to substrate carbon. The maximum decomposition rate  $V_{max}$  varied with temperature according to the Arrhenius relationship:

$$V_{max,i}(T) = V_{max,ref,i} \times \exp\left(-\frac{E_{a,i}}{RT}\right) \quad (11)$$

where  $V_{max,ref,i}$  is a maximum decomposition rate parameter specific to each chemically defined organic matter type,  $E_{a,i}$  is activation energy for each organic matter type, and  $R$  is the ideal gas constant (8.31 J·K<sup>-1</sup>·mol<sup>-1</sup>).

Microbial biomass in the model had a fixed C:N ratio. Microbial growth ( $G_M$ ) was supported by uptake of decomposed organic matter, and biomass was lost via turnover at a first order rate limited by a minimum allowed microbial biomass:

$$\frac{dC_M}{dt} = G_M - \frac{\max(C_M - C_{M,min} * \sum_i C_{U,i}, 0)}{\tau_{mic}} \quad (12)$$

$$\frac{dN_M}{dt} = \frac{1}{C:N_m} \frac{dC_M}{dt} \quad (13)$$

Where  $C_{M,min}$  is minimum microbial biomass C expressed as a fraction of total unprotected C. Turnover was divided into maintenance respiration ( $R_{maint}$ ), which was converted directly to CO<sub>2</sub>, and necromass production. Microbial necromass was divided into quickly cycling organic matter and chemically resistant organic matter. The division between maintenance respiration and necromass production was controlled by a parameter  $\epsilon_t$ :

$$R_{maint} = \frac{\max(C_M - C_{M,min} * \sum_i C_{U,i}, 0)}{\tau_{mic}} (1 - \epsilon_t) \quad (14)$$

Limitation of microbial growth by N versus C was determined by a nitrogen balance term, which reflected carbon and nitrogen assimilation through decomposition in the context of the microbial C:N ratio:

$$\Phi_N = \sum_i (\epsilon_{N,i} D_{N,i}) - (\sum_i (\epsilon_{C,i} D_{C,i}) - R_{\text{maint}}) / C:N_M \quad (15)$$

Here,  $\epsilon_{N,i}$  is the N uptake efficiency for each organic matter type,  $\epsilon_{C,i}$  is the C uptake efficiency for each organic matter type, and  $R_{\text{maint}}$  is the microbial maintenance respiration. When  $\Phi_N$  was zero, carbon and nitrogen uptake were balanced. When  $\Phi_N$  was greater than zero, carbon uptake was not sufficient to balance nitrogen uptake and excess nitrogen was mineralized. When  $\Phi_N$  was less than zero, nitrogen uptake was not sufficient to balance carbon uptake and inorganic nitrogen was immobilized. When the need for nitrogen exceeded the maximum immobilization rate  $Imm_{\text{max}}$ , growth was limited by available nitrogen:

$$G_M = \begin{cases} \sum_i \{ \epsilon_{C,i} \{ D_{C,i} + D_{C,i,\text{denit}} \}, \Phi_N \geq -Imm_{\text{max}} \\ C:N_M \cdot \{ \sum_i \{ \epsilon_{N,i} \{ D_{N,i} + D_{N,i,\text{denit}} \} + Imm_{\text{max}} + R_{\text{maint}} \}, \Phi_N < -Imm_{\text{max}} \end{cases} \quad (16)$$

The inorganic N pool was divided into ammonium ( $\text{NH}_4^+$ ) and nitrate ( $\text{NO}_3^-$ ). Fluxes to and from these pools included exchanges with microbes through mineralization and immobilization, uptake by plants ( $N_{\text{up,veg}}$  for each type of inorganic N), and net leaching ( $L$ ).  $\text{NH}_4^+$  was produced from OM mineralization as a byproduct of decomposition.  $\text{NH}_4^+$  was converted to  $\text{NO}_3^-$  through nitrification ( $Nit$ ), and  $\text{NO}_3^-$  was lost to the atmosphere through denitrification ( $Denit$ ). Inorganic N was also added through atmospheric deposition ( $N_{\text{dep}}$ ).  $\text{NO}_3^-$  and  $\text{NH}_4^+$  were taken up by immobilization when microbial growth was limited, and this uptake was partitioned between the two inorganic N species based on the amount of each weighted by a chemical-specific microbial immobilization rate ( $V_{\text{NH}_4}$  and  $V_{\text{NO}_3}$ ).

$$\frac{d\text{NH}_4}{dt} = \begin{cases} \Phi_N + (1 - \epsilon_{N,i}) (D_{N,i} + D_{N,i,\text{denit}}) - Nit + N_{\text{dep},\text{NH}_4} + L_{\text{NH}_4} - N_{\text{up,veg},\text{NH}_4}, \Phi_N > 0 \\ \Phi_N \frac{V_{\text{NH}_4} \text{NH}_4}{V_{\text{NH}_4} \text{NH}_4 + V_{\text{NO}_3} \text{NO}_3} + (1 - \epsilon_{N,i}) (D_{N,i} + D_{N,i,\text{denit}}) - Nit + N_{\text{dep},\text{NH}_4} + L_{\text{NH}_4} - N_{\text{up,veg},\text{NH}_4}, 0 > \Phi_N > -Imm_{\text{max}} \\ -Imm_{\text{max}} \frac{V_{\text{NH}_4} \text{NH}_4}{V_{\text{NH}_4} \text{NH}_4 + V_{\text{NO}_3} \text{NO}_3} + (1 - \epsilon_{N,i}) (D_{N,i} + D_{N,i,\text{denit}}) - Nit + N_{\text{dep},\text{NH}_4} + L_{\text{NH}_4} - N_{\text{up,veg},\text{NH}_4}, \Phi_N < -Imm_{\text{max}} \end{cases} \quad (17)$$

$$\frac{d\text{NO}_3}{dt} = \begin{cases} Nit - Denit + N_{\text{dep},\text{NO}_3} + L_{\text{NO}_3} - N_{\text{up,veg},\text{NO}_3}, \Phi_N > 0 \\ \Phi_N \frac{V_{\text{NO}_3} \text{NO}_3}{V_{\text{NH}_4} \text{NH}_4 + V_{\text{NO}_3} \text{NO}_3} + Nit - Denit + N_{\text{dep},\text{NO}_3} + L_{\text{NO}_3} - N_{\text{up,veg},\text{NO}_3}, 0 > \Phi_N > -Imm_{\text{max}} \\ -Imm_{\text{max}} \frac{V_{\text{NO}_3} \text{NO}_3}{V_{\text{NH}_4} \text{NH}_4 + V_{\text{NO}_3} \text{NO}_3} + Nit - Denit + N_{\text{dep},\text{NO}_3} + L_{\text{NO}_3} - N_{\text{up,veg},\text{NO}_3}, \Phi_N < -Imm_{\text{max}} \end{cases} \quad (18)$$

When microbial growth was N limited, excess C taken up from decomposition was converted to  $\text{CO}_2$  through overflow respiration:

$$R_{\text{overflow}} = \begin{cases} 0, \Phi_N \geq -Imm_{\text{max}} \\ -(\Phi_N + Imm_{\text{max}}) C:N_M, \Phi_N < -Imm_{\text{max}} \end{cases} \quad (19)$$

Total  $\text{CO}_2$  production rate was the sum of maintenance respiration, overflow respiration, and respiration derived from decomposition processes:

$$F_{\text{CO}_2} = R_{\text{maint}} + R_{\text{overflow}} + \sum_i ((1 - \epsilon_{C,i}) D_{C,i}) \quad (20)$$

Nitrification occurred at a temperature- and moisture-dependent first-order rate:

$$Nit = V_{\text{nit}}(T) \left( \frac{\theta}{\theta_{\text{sat}}} \right)^3 \left( 1 - \frac{\theta}{\theta_{\text{sat}}} \right)^{2.5} \text{NH}_4 \quad (21)$$

OM decomposition through denitrification was calculated similarly to aerobic decomposition, but with a lower  $V_{\max}$  and a moisture dependence that increased at high moisture levels rather than peaking at moderate moisture:

$$D_{C,i,\text{denit,pot}} = V_{\max,i,\text{denit}}(T) \cdot \left(\frac{\theta}{\theta_{\text{sat}}}\right)^{5.5} \frac{1}{f_{\theta,\max}} \cdot C_{U,i} \frac{\frac{C_M}{C_{U,i}}}{\frac{C_M}{C_{U,i}} + k_M} \quad (22)$$

$$D_{N,i,\text{denit,pot}} = V_{\max,i,\text{denit}}(T) \cdot \left(\frac{\theta}{\theta_{\text{sat}}}\right)^{5.5} \frac{1}{f_{\theta,\max}} \cdot N_{U,i} \frac{C_M/C_{U,i}}{C_M/C_{U,i} + k_M} \quad (23)$$

where  $D_{C,i,\text{denit,pot}}$  and  $D_{N,i,\text{denit,pot}}$  are potential denitrification-supported decomposition rates for C and N, respectively.  $\text{NO}_3^-$  demand due to denitrification was calculated using a stoichiometry-determined ratio of 0.93 g N/g C decomposed ( $f_{\text{den}}$ ) (Heinen, 2006) and denitrification-supported decomposition was limited by nitrate availability:

$$D_{C,i,\text{denit}} = D_{C,i,\text{denit,pot}} \cdot \text{NO}_3^- / (\text{NO}_3^- + k_{\text{denit}} \sum_i D_{C,i,\text{denit,pot}} \cdot f_{\text{den}}) \quad (24)$$

$$D_{N,i,\text{denit}} = D_{N,i,\text{denit,pot}} \cdot \text{NO}_3^- / (\text{NO}_3^- + k_{\text{denit}} \sum_i D_{C,i,\text{denit,pot}} \cdot f_{\text{den}}) \quad (25)$$

$$\text{Denit} = D_{C,i,\text{denit}} \cdot f_{\text{den}} \quad (26)$$

Leaching transfers of OM,  $\text{NO}_3^-$ , and  $\text{NH}_4^+$  between soil layers were calculated using water flows provided by the LM3 hydrology model (Milly et al., 2014). A solubility parameter specific to each OM or inorganic N type determined the fraction of the pool that could be transferred in each time step, and the dissolved fraction was transported between soil layers along with water flow. Water flow out of the soil column due to vertical divergence of the flow pattern carried dissolved material out of the column as belowground runoff.

### 2.1.3. Plant N Uptake Strategies

Plant N acquisition in the model occurred through four pathways: (1) root uptake of inorganic N in the rhizosphere; (2) scavenging of inorganic N by AM, (3) mining of N via decomposition of OM by ericoid or ectomycorrhizae, and (4) symbiotic  $\text{N}_2$  fixation.

#### 2.1.3.1. Direct N Uptake by Roots

Direct N uptake by roots in the model occurred through two processes: First, as roots took up soil water they also absorbed the dissolved N contained in the soil water (passive N uptake). The flux of passive inorganic N uptake was the concentration of N in soil water multiplied by the root water uptake flux:

$$\text{NO}_{3,\text{passive}}(k) = U(k) \cdot \frac{\text{NO}_3(k)}{\text{H}_2\text{O}(k)} \quad (27)$$

$$\text{NH}_{4,\text{passive}}(k) = U(k) \cdot \frac{\text{NH}_4(k)}{\text{H}_2\text{O}(k)} \quad (28)$$

where  $k$  is the soil layer,  $\text{NO}_{3,\text{passive}}$  and  $\text{NH}_{4,\text{passive}}$  are passive N uptake fluxes ( $\text{kg N} \cdot \text{m}^{-2} \cdot \text{s}^{-1}$ ),  $U$  is the root water uptake flux ( $\text{kg} \cdot \text{m}^{-2} \cdot \text{s}^{-1}$ ),  $\text{NO}_3^-$  and  $\text{NH}_4^+$  are the pools of nitrate and ammonium in the soil layer, respectively ( $\text{kg N} \cdot \text{m}^{-2}$ ), and  $\text{H}_2\text{O}$  is the water content of the layer ( $\text{kg/m}^2$ ).

Roots also absorbed soil N using active transport mechanisms. This N uptake process was limited by the rhizosphere volume accessible to fine roots, but did not depend on the rate of water movement from the soil into roots:

$$\text{NO}_{3,\text{active}}(k) = f_{\text{rhiz}}(k) \cdot r_{\text{NO}_3} \cdot \frac{\text{NO}_3(k)/\Delta z(k)}{\text{NO}_3(k)/\Delta z(k) + k_{M,\text{NO}_3}} \quad (29)$$

$$\text{NH}_{4,\text{active}}(k) = f_{\text{rhiz}}(k) \cdot r_{\text{NH}_4} \cdot \frac{\text{NH}_4(k)/\Delta z(k)}{\text{NH}_4(k)/\Delta z(k) + k_{M,\text{NH}_4}} \quad (30)$$

where  $\Delta z$  is the layer thickness,  $\text{NO}_{3,\text{active}}$  and  $\text{NH}_{4,\text{active}}$  are active root N uptake rates,  $f_{\text{rhiz}}$  is rhizosphere fraction of the soil layer, and  $r_{\text{NH}_4}$  and  $r_{\text{NO}_3}$  are rate constants for ammonium and nitrate, respectively.



$f_{\text{rhiz}}$  was calculated using volumetric root length and mean root and rhizosphere radius (Finzi et al., 2015) and therefore directly depended on root biomass and morphology:

$$f_{\text{rhiz}}(k) = \pi((r_{\text{rhiz}} + r_{\text{root}})^2 - r_{\text{root}}^2) \cdot \text{VRL}(k) \quad (31)$$

where  $r_{\text{rhiz}}$  is the radius of the rhizosphere around the root,  $r_{\text{root}}$  is the radius of the root, and  $\text{VRL}$  is volumetric root length in the soil layer.

### 2.1.3.2. Inorganic N Scavenging by Mycorrhizal Fungi

Compared to root uptake, AM mycorrhizal scavenging accessed a larger soil volume and had a higher potential uptake rate. Mycorrhizal scavenging of N occurred in all soil layers as well as the litter layer. The rate of N uptake in each layer had a Michaelis–Menten type saturating dependence on both inorganic N concentration and mycorrhizal biomass concentration in the layer:

$$N_{\text{scav},\text{NO}_3}(k) = V_{\text{scav}} \cdot \frac{\frac{\text{NO}_3(k)}{\Delta z(k)}}{\frac{\text{NO}_3(k)}{\Delta z(k)} + k_{\text{scav},\text{Ninorg}}} \cdot \frac{\frac{B_{\text{scav}}(k)}{\Delta z(k)}}{\frac{B_{\text{scav}}(k)}{\Delta z(k)} + k_{\text{scav}}} \quad (32)$$

$$N_{\text{scav},\text{NH}_4}(k) = V_{\text{scav}} \cdot \frac{\frac{\text{NH}_4(k)}{\Delta z(k)}}{\frac{\text{NH}_4(k)}{\Delta z(k)} + k_{\text{scav},\text{Ninorg}}} \cdot \frac{\frac{B_{\text{scav}}(k)}{\Delta z(k)}}{\frac{B_{\text{scav}}(k)}{\Delta z(k)} + k_{\text{scav}}} \quad (33)$$

where  $N_{\text{scav}}$  is the rate of nitrogen uptake by mycorrhizal scavengers,  $V_{\text{scav}}$  is a rate constant,  $B_{\text{scav}}$  is scavenger mycorrhizal biomass in the layer, and  $k_{\text{scav}}$  and  $k_{\text{scav},\text{Ninorg}}$  are the half-saturation constants for mycorrhizal biomass and inorganic N concentration, respectively. The model partitioned mycorrhizal biomass among layers using the vertical root biomass profile, assuming that roots and mycorrhizae had the same vertical profiles.

### 2.1.3.3. Organic N Mining by Mycorrhizal Fungi

Mining (ECM and ericoid) mycorrhizae decomposed SOM at a rate depending on the mycorrhizal biomass pool, using similar relationships to those used for OM decomposition in the CORPSE-N model. As with scavenging mycorrhizae, the model simulated total mining mycorrhizal biomass and divided it among layers based on the root profile. Mining mycorrhizae took up both C and N from the organic matter that they decomposed:

$$D_{C,i,\text{mine}}(k) = V_{\text{max},i,\text{mine}}(T) \cdot \left(\frac{\theta}{\theta_{\text{sat}}}\right)^3 \left(1 - \frac{\theta}{\theta_{\text{sat}}}\right)^{2.5} \frac{1}{f_{\theta,\text{max}}} \cdot C_{U,i}(k) \frac{B_{\text{mine}}(k)/C_{U,i}(k)}{B_{\text{mine}}(k)/C_{U,i}(k) + k_{M,\text{mine}}} \quad (34)$$

$$D_{N,i,\text{mine}}(k) = V_{\text{max},i,\text{mine}}(T) \cdot \left(\frac{\theta}{\theta_{\text{sat}}}\right)^3 \left(1 - \frac{\theta}{\theta_{\text{sat}}}\right)^{2.5} \frac{1}{f_{\theta,\text{max}}} \cdot N_{U,i}(k) \frac{B_{\text{mine}}(k)/C_{U,i}(k)}{B_{\text{mine}}(k)/C_{U,i}(k) + k_{M,\text{mine}}} \quad (35)$$

$$\text{CO}_{2\text{mine}}(k) = \sum_i D_{C,i,\text{mine}}(k) \cdot (1 - \epsilon_{C,i,\text{mine}}) \quad (36)$$

$$N_{\text{mine}}(k) = \sum_i D_{N,i,\text{mine}}(k) \cdot \epsilon_{N,i,\text{mine}} \quad (37)$$

$$C_{\text{mine}}(k) = \sum_i D_{C,i,\text{mine}}(k) \cdot \epsilon_{C,i,\text{mine}} \quad (38)$$

where  $C_{\text{mine}}$  is C uptake by miners,  $N_{\text{mine}}$  is N uptake by miners,  $\text{CO}_{2\text{mine}}$  is carbon dioxide produced in the mining process,  $B_{\text{mine}}$  is miner mycorrhizal biomass in the layer,  $T$  is soil temperature,  $\theta$  is soil moisture,  $\theta_{\text{sat}}$  is saturation soil moisture, and  $\epsilon_{C,i,\text{mine}}$  and  $\epsilon_{N,i,\text{mine}}$  are the C and N uptake efficiency of miner mycorrhizae, respectively.

### 2.1.3.4. Symbiotic N<sub>2</sub> Fixation

The symbiotic N fixation rate was directly proportional to the biomass of N<sub>2</sub> fixers, and had a temperature dependence function based on Houlton et al. (2008):

$$N_{\text{fix}} = r_{\text{fix}} \cdot B_{\text{fix}} e^{-3.4 + 0.27(T_s(1 - 0.02T_s))} \quad (39)$$

where  $N_{\text{fix}}$  is nitrogen fixation rate,  $r_{\text{fix}}$  is a rate constant,  $T_s$  is soil temperature in C, and  $B_{\text{fix}}$  is biomass of nitrogen fixing microbes. Note that this temperature dependence was not developed in the specific context of symbiotic N fixation, and may require revision in the future.

#### 2.1.4. Growth and Turnover of Symbiotic Biomass

C and N acquired by mycorrhizae and N<sub>2</sub> fixing bacteria as well as plant C and N allocated to symbionts were transferred to intermediate C and N pools. Symbiont biomass accumulation and N transfers to plants were both calculated using the intermediate pools. Because symbiont growth depleted this N pool, under N-limited conditions transfers to plants could be reduced due to mycorrhizal immobilization of nitrogen. Symbionts converted C into biomass with a fixed efficiency specific to each symbiont type. The remaining carbon was converted to CO<sub>2</sub>. Strategies with higher C costs (such as N<sub>2</sub> fixation) had lower efficiencies. The C:N ratio of symbiont biomass was fixed and biomass accumulation of scavenging and mining mycorrhizae was limited when not enough N was available, here defined as depleting more than 90% of the intermediate N pool within a single 30-min time step (dt):

$$G_j = \min \left( \frac{r_{\text{growth}} C_{\text{int},j}}{(C_{\text{int},j} + k_G)} \epsilon_j, \frac{N_{\text{int},j}}{dt} \cdot 0.9 \cdot C:N_j + \frac{B_j}{\tau_j} (1 - e_{t,\text{sym}}) \right) \quad (40)$$

where  $G_j$  is symbiotic biomass growth rate for strategy  $j$  (scavenging, mining, or N<sub>2</sub> fixation),  $B_j$  is symbiotic biomass,  $r_{\text{growth}}$  is the maximum symbiont growth rate (assumed to be the same for all strategies),  $k_G$  is the half-saturation constant for symbiont growth,  $\epsilon_j$  is the growth efficiency,  $\tau_j$  is the turnover time for symbiotic biomass,  $e_{t,\text{sym}}$  is the fraction of symbiotic biomass turnover not used for maintenance respiration, and  $C_{\text{int},j}$  and  $N_{\text{int},j}$  are the intermediate C and N pools, respectively. N fixing bacteria were assumed to fix the N they needed for their own biomass and their growth was therefore not N limited. Symbiont biomass turned over at a fixed, first-order rate, returning a fraction of biomass N to the intermediate pool:

$$\frac{dB_j}{dt} = G_j - \frac{B_j}{\tau_j} \quad (41)$$

Intermediate pools supported symbiont growth as well as transfers to plants, and lost C to root exudate leakage at a fixed time scale  $\tau_{\text{int}}$ :

$$\frac{dC_{\text{int},\text{mine}}}{dt} = C_{\text{transfer},\text{mine}} + C_{\text{mine}} - \frac{G_{\text{mine}}}{\epsilon_{\text{mine}}} - \frac{C_{\text{int},\text{mine}}}{\tau_{\text{int}}} \quad (42)$$

$$\frac{dC_{\text{int},\text{scav}}}{dt} = C_{\text{transfer},\text{scav}} - \frac{G_{\text{scav}}}{\epsilon_{\text{scav}}} - \frac{C_{\text{int},\text{scav}}}{\tau_{\text{int}}} \quad (43)$$

$$\frac{dC_{\text{int},\text{fix}}}{dt} = C_{\text{transfer},\text{fix}} - r_{\text{growth}} \frac{C_{\text{int},\text{fix}}}{C_{\text{int},\text{fix}} + k_G} - \frac{C_{\text{int},\text{fix}}}{\tau_{\text{int}}} \quad (44)$$

$$\frac{dN_{\text{int},\text{mine}}}{dt} = N_{\text{transfer},\text{mine}} + N_{\text{mine}} - \frac{1}{C:N_{\text{mine}}} \frac{G_{\text{mine}}}{\epsilon_{\text{mine}}} - N_{\text{int},\text{mine}} r_{\text{up,veg}} + \frac{B_{\text{mine}}}{C:N_{\text{mine}} \tau_{\text{mine}}} (1 - e_{t,\text{sym}}) \quad (45)$$

$$\frac{dN_{\text{int},\text{scav}}}{dt} = N_{\text{transfer},\text{scav}} + N_{\text{scav}} - \frac{1}{C:N_{\text{scav}}} \frac{G_{\text{scav}}}{\epsilon_{\text{scav}}} - N_{\text{int},\text{scav}} r_{\text{up,veg}} + \frac{B_{\text{scav}}}{C:N_{\text{scav}} \tau_{\text{scav}}} (1 - e_{t,\text{sym}}) \quad (46)$$

$$\frac{dN_{\text{int},\text{fix}}}{dt} = N_{\text{fix}} - N_{\text{int},\text{fix}} r_{\text{up,veg}} \quad (47)$$

where  $r_{\text{up,veg}}$  is the rate of plant N uptake from the intermediate pool. C and N from turnover of symbiont biomass was added to the soil as microbial necromass carbon, with a vertical profile determined by the root profile.

## 2.2. Site Comparisons and Model Simulations

To evaluate the model against contrasting responses of AM- and ECM-dominated ecosystems to elevated CO<sub>2</sub> (Objective 1), we ran simulations for two forest FACE experiments that differed in mycorrhizal association: Duke (Drake et al., 2011; Finzi et al., 2001) and Oak Ridge National Laboratory (Norby et al., 2002). The Duke experiment was conducted in a loblolly pine (*Pinus taeda* L.) forest initiated in 1983 in North Carolina, USA. The soils are classified as low-fertility Ustic Hapludalfs of the Enon series, the mean annual temperature is 15.5 °C and the mean annual precipitation is 1,140 mm (Schlesinger et al., 2006). The Oak Ridge National Laboratory (ORNL) experiment was conducted in a sweetgum (*Liquidambar styraciflua* L.)

plantation initiated in 1988 in Tennessee, USA. The soils are classified as Aquic Hapludults (Jastrow et al., 2005), the mean annual temperature is 13.9 °C, and the mean annual precipitation is 1,371 mm (Warren et al., 2011). Simulations used the published protocol and meteorological driving data from the Phase 1 FACE Model-Data Synthesis (Norby et al., 2015). The model was spun up for 400 years using repeated meteorology from the protocol. Site-specific land use history was then used to conduct historical simulations for each site from the year 1700 through the establishment of the FACE experiments (1996 for Duke and 1998 for ORNL). N acquisition strategies for each site were determined by the mycorrhizal association of the dominant tree type. Duke, an ECM-associated loblolly pine plantation, was simulated as an evergreen forest that used the ECM N mining strategy. ORNL, an AM-associated sweetgum plantation, was simulated as a deciduous forest using the AM N scavenging strategy. Along with different N acquisition strategies, the forests differed in leaf and fine root C:N ratios, N retranslocation fractions, litter labile OM fraction, leaf thickness, and partitioning of growth among wood, leaves, and roots. These parameters were all determined using site-specific data where possible, and data specific to tree species or functional type (evergreen needleleaf vs. deciduous broadleaf) where site-specific measurements were unavailable. Simulations with ambient and elevated levels of CO<sub>2</sub> using measured values from the published protocol were then conducted for each site. Symbiotic N<sub>2</sub> fixation was not active in simulations for either site following forest establishment. See Table S2 for the full table of model parameters and Table S1 for differences in parameterization between sites.

To estimate the sensitivity of the model and results to poorly constrained parameters, we conducted a sensitivity analysis using ecosystem-scale simulations targeted at key parameters controlling mycorrhizal growth and N acquisition rates. Simulations to assess parameter sensitivity began at the initiation of forest vegetation (as determined by site history for Duke and ORNL). For each parameter, we conducted two additional simulations in which the parameter value was increased and decreased by 25%, respectively. These simulations were conducted for  $V_{\text{scav}}$ ,  $V_{\text{max,ref,mine}}$  (with the same percent change applied to the value for each organic matter type),  $\tau_{\text{scav}}$ , and  $\tau_{\text{mine}}$ .  $\tau_{\text{scav}}$  and  $\tau_{\text{mine}}$  affected the relationship between  $C_{\text{transfer}}$  and mycorrhizal biomass in similar ways to  $\epsilon_{\text{scav}}$  and  $\epsilon_{\text{mine}}$ . We were unable to conduct sensitivity analyses at global scales for this study due to the computational resources required.

Ecosystem-scale simulations were compared with observations extracted from publications from the two FACE experiments. Duke soil observations were taken from Table 4 and Figure 1b in Lichter et al. (2008) and Table 3 in Lichter et al. (2005). ORNL soil observations were taken from Table 1 in Iversen et al. (2012). Vegetation biomass measurements for both sites and N uptake estimates for Duke (Figure 1b) used the synthesis data set of Finzi et al. (2007) as available at <https://facedata.ornl.gov/synthesis/>. N uptake estimates for ORNL are from Norby et al. (2010). Error bars in Figures 2 and 3 show the reported error ranges from the original publications.

We used global simulations to evaluate global patterns of N acquisition (Objective 2) and their responses to an increase in CO<sub>2</sub> levels (Objective 3). Global simulations were driven using years 1948–1978 of gridded historical meteorological forcing (Sheffield et al., 2006), repeated to run simulations of arbitrary length. The model was spun up until C and N pools reached approximate steady state (about 1,000 years). Spinup and control simulations used atmospheric CO<sub>2</sub> concentrations of 286 ppm. Atmospheric N deposition was applied using the estimates of Green et al. (2004). Spinup used preindustrial N deposition estimates. Modern N deposition was then applied for 100 years before starting the elevated CO<sub>2</sub> manipulations. For elevated CO<sub>2</sub> simulations, the atmospheric CO<sub>2</sub> level was raised as a step change from 286 to 386 ppm and compared to simulations in which CO<sub>2</sub> concentration was held constant at 286 ppm. We chose to simulate a step change rather than more gradual historical and projected CO<sub>2</sub> concentrations to make the global simulations more comparable to site-scale experiments and to allow the analysis to focus on ecosystem dynamics rather than historical patterns. All simulations used identical climate forcing. We simulated three scenarios of vegetation N acquisition responses: One in which  $f_{\text{alloc}}$  and  $C_{\text{transfer}}$  changed dynamically in response to changing N demand (dynamic symbiotic allocations), one in which  $f_{\text{alloc},j}$  and  $C_{\text{transfer}}$  were held constant but plant growth could be limited by N availability (static symbiotic allocations), and one in which plant growth was not N limited and  $f_{\text{alloc}}$  and  $C_{\text{transfer}}$  did not respond to changes in N availability or demand (no N limitation). Static symbiotic allocations were simulated by applying a smoothing filter with a time scale of 1,000 years to  $f_{\text{alloc},j}$  for all strategies. A 1,000 year smoothing filter was also applied to N stress to

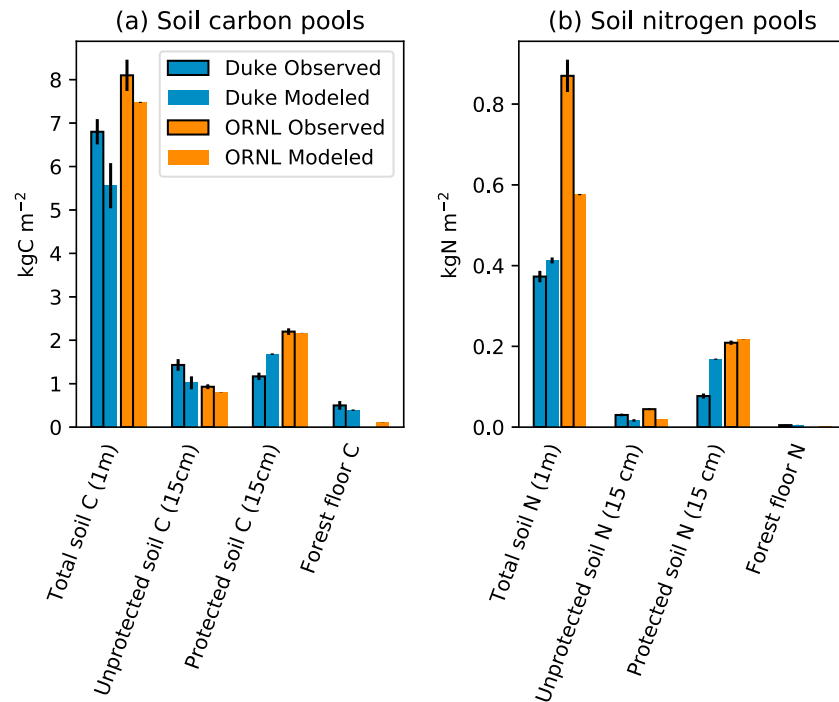


**Figure 2.** Modeled and observed soil C and N pools for the two FACE experiments. Modeled values are averaged over the year prior to initiation of the elevated CO<sub>2</sub> treatment. Soil observations for Duke are from control plots with totals to 1 m measured in 2005, forest floor measured in 1996, and fractions to 15 cm measured in 1996 and 1999 (Lichter et al., 2005, 2008). ORNL soil measurements were from control plots and were collected in 2009 (Iversen et al., 2012). Error bars show reported error from observation source publications for observations and variability across the sensitivity analysis for the model. Note that this is not a comprehensive estimate of model uncertainty. FACE = free air carbon enrichment; ORNL = Oak Ridge National Laboratory.

prevent  $C_{transfer}$  from changing. The no N limitation scenario was simulated by holding  $N_{stress}$  constant so that  $C_{transfer}$  was a constant fraction of NPP. In this scenario,  $N_{storage}$  was allowed to be less than zero and plant tissue growth was not limited by N availability.

### 2.3. Mycorrhizal Species Distribution Models

To determine if modeled AM and ECM distributions were congruous with observed distributions of these fungal guilds we compared a novel, empirical niche-based species distribution model of fungal guild distributions with those generated by our global model. Empirical AM data points were obtained from the MAARJAM database (Öpik et al., 2010, accessed 2 February 2018), and ECM data points were obtained from Tedersoo et al. (2014). We compared modeled mycorrhizal biomass with empirical presence/absence observations using a cutoff of mean annual modeled mycorrhizal biomass greater than 5 g C/m<sup>2</sup>. Niche models were created using the Maxent algorithm (Phillips et al., 2006) and validated against overfitting and accuracy via the ENMEval R package (Muscarella et al., 2014) following Kivlin et al. (2017). We compared the niche overlap of model-based and empirical-based AM or ECM distributions using the calc.niche.overlap function in the ENMEval R package with the I similarity statistic (Warren et al., 2008).

## 3. Results

### 3.1. Ecosystem-Scale Simulations

We first conducted and evaluated LM3-SNAP simulations at the ecosystem scale using the rich data sets from two forest FACE experiments that differed in mycorrhizal association: Duke (ECM-dominated) and ORNL (AM-dominated). Soil and forest floor C and N stocks at the beginning of the elevated CO<sub>2</sub> treatments were generally consistent with available observations from both Duke (Lichter et al., 2005, 2008) and ORNL (Iversen et al., 2012), although the model underestimated total soil N at ORNL and overestimated protected soil N at Duke (Figure 2). Forest floor and unprotected C stocks were higher in the Duke simulation than in

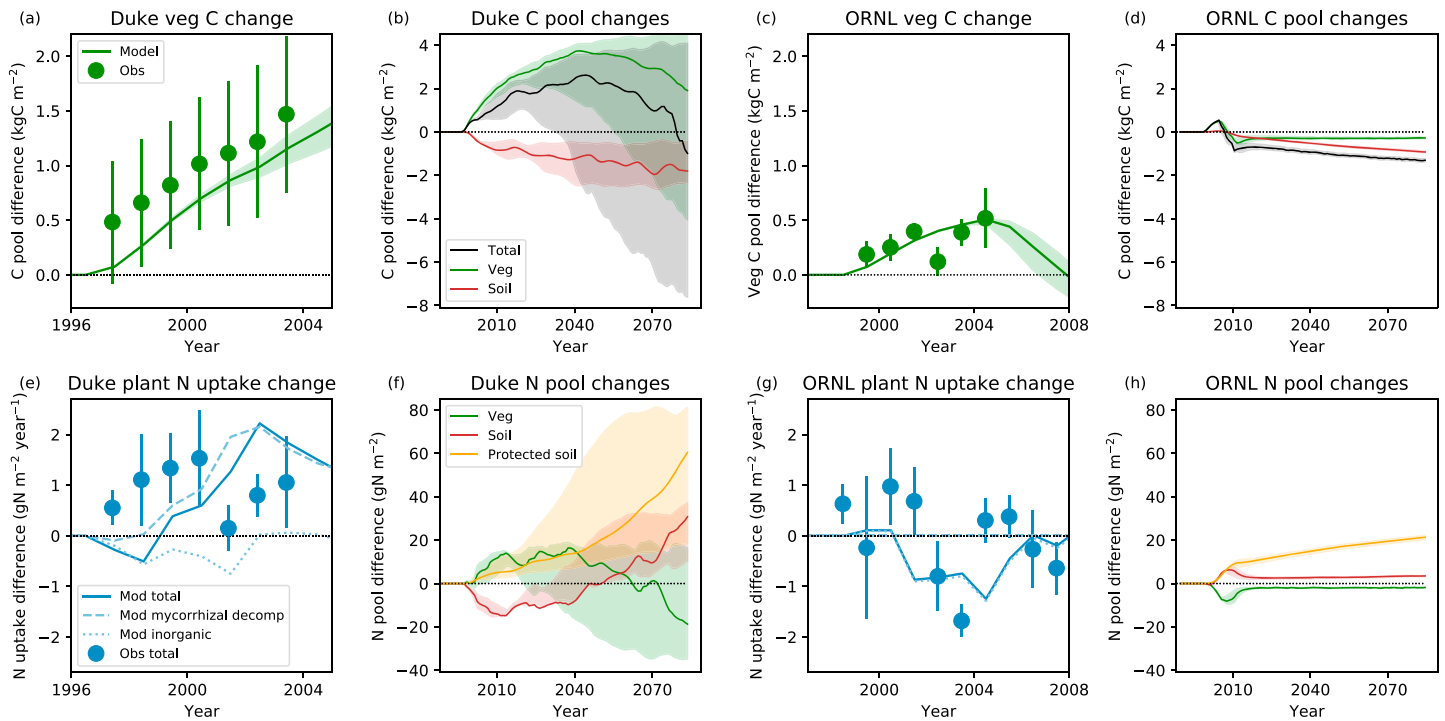


**Figure 3.** Carbon and nitrogen responses to elevated  $\text{CO}_2$ . (a): Modeled and measured annual differences in vegetation biomass C between elevated and ambient  $\text{CO}_2$  in the Duke experiment. (b): Vegetation and soil C differences over long-term simulations of the Duke experiment. Shading shows the range across the sensitivity analysis. (c): Modeled and measured annual differences in vegetation biomass C between elevated and ambient  $\text{CO}_2$  in the Oak Ridge National Laboratory (ORNL) experiment. (d): Vegetation and soil C differences over long-term simulations of the ORNL experiment. (e): Modeled and measurement-based annual differences in N uptake between elevated and ambient  $\text{CO}_2$  in the Duke experiment. Dashed lines show N uptake via soil organic matter decomposition and dotted lines show uptake of inorganic N. (f): Protected soil N, total soil N, and vegetation N differences over long-term simulations of the Duke experiment. Shading shows the range across the sensitivity analysis. (g): Modeled and measurement-based annual differences in N uptake between elevated and ambient  $\text{CO}_2$  in the ORNL experiment. (h): Protected soil N, total soil N, and vegetation N differences over long-term simulations of the ORNL experiment.

the ORNL simulation due to decomposition-resistant litter properties associated with the Duke pine forest. Protected C and N stocks were larger at ORNL than at Duke because ORNL litter had a higher labile fraction (with a higher microbial carbon use efficiency converting more litter material to microbial necromass) and ORNL soil had a higher clay content (driving more rapid protected SOM formation), but the model underestimated the contrast between sites relative to observations.

Comparing differences in plant biomass and N uptake between control and elevated  $\text{CO}_2$  treatments, LM3-SNAP was able to reproduce the contrasting responses to elevated  $\text{CO}_2$  observed at these sites (Figures 3a, 3c, 3e, and 3g). As an ECM-dominated site, Duke could accelerate turnover of litter and SOM pools via enhanced allocation of C to ECM under elevated  $\text{CO}_2$ , allowing it to increase N uptake by 1–2  $\text{g N m}^{-2} \cdot \text{year}^{-1}$  (Figure 3e, dashed lines). The increase in total N uptake was entirely due to mycorrhizal N mining—N uptake from inorganic sources did not increase significantly, and in fact decreased relative to control in some years. In contrast to Duke, vegetation at ORNL, an AM-dominated site which relied on soil inorganic N, rapidly became N limited because soil inorganic N availability did not increase in response to higher plant N demand (Figure 3g). As a result, vegetation at ORNL accrued little additional biomass under elevated  $\text{CO}_2$  (Figure 3c).

While the elevated  $\text{CO}_2$  manipulations at the experimental sites only lasted on the order of 10 years, we continued model simulations for an additional 75 years to investigate long-term outcomes. In simulations with the baseline parameters, the Duke site continued to accumulate vegetation biomass over approximately 40 years, peaking at almost 4  $\text{kg C/m}^2$  more than control (Figure 3b). This growth was supported by a transfer of 10–15  $\text{g/m}^2$  of N from soil into vegetation (Figure 3f), which also reduced soil C by 1–2  $\text{kg C/m}^2$  (Figure 3b). However, this accumulation of C under elevated  $\text{CO}_2$  was ultimately temporary except in simulations with increased mycorrhizal decomposition rates ( $V_{\text{max,ref,mine}}$ ). The long-term enhancement of root

exudation and mycorrhizal subsidies at the Duke site also accelerated N immobilization in microbial biomass, which trapped increasing amounts of N in protected SOM pools via physico-chemical stabilization of microbially processed material (Bingham & Cotrufo, 2016; Cotrufo et al., 2013) (Figure 3f, yellow line). This increase in protected soil N reduced the amount of bioavailable soil N, ultimately limiting the ability of vegetation to accumulate more N under elevated CO<sub>2</sub> relative to control treatments (Figure 3f, green line). Combined with soil C losses driven by priming of decomposition, the declining vegetation growth enhancement caused the elevated CO<sub>2</sub> treatment to lose C relative to the control treatment after 80 years in baseline simulations and after 40 years in simulations with reduced  $V_{\max,\text{ref,mine}}$ , while simulations with increased  $V_{\max,\text{ref,mine}}$  were able to maintain enhanced C accumulation for the length of the simulation (Figures 3b and S1a).

In contrast to the changing trajectory of C and N pools at the Duke site, the long-term response of the ORNL site was substantially weaker, more steady over time, and less sensitive to mycorrhizal parameters (Figures S1 and 3d). While vegetation C initially accumulated faster under elevated CO<sub>2</sub>, vegetation C eventually stabilized at a slightly lower value than control as N limitation became more important. Approximately 15 g N/m<sup>2</sup> was trapped in protected SOM pools over the first 20–30 years of elevated CO<sub>2</sub>, leading to a slight decline in total vegetation N and a slight increase in total soil N (Figure 3h). After the initial few years, simulated total C at the ORNL site decreased under elevated CO<sub>2</sub> relative to control (Figure 3d).

Sensitivity analysis simulations showed substantial differences in parameter sensitivity between the Duke and ORNL sites. C and N stock responses to elevated CO<sub>2</sub> at ORNL were insensitive to changes in mycorrhizal N uptake and biomass turnover parameters, with C and N stocks changing by less than 0.1 kg C/m<sup>2</sup> and 0.5 g N/m<sup>2</sup>, respectively (Figures 3d, 3h, and S1). This insensitivity to mycorrhizal parameters indicates that ecosystem responses were driven by inorganic N availability rather than by mycorrhizal uptake rates. By contrast, trajectories of both C and N pools at Duke were highly sensitive to  $V_{\max,\text{ref,mine}}$  and  $\tau_{\text{mine}}$  (Figures 3b, 3f, and S1). The 25% decreases in these parameters, which made mycorrhizal decomposition and N acquisition less efficient, caused vegetation C accumulation under elevated CO<sub>2</sub> to end up to 20 years sooner, while tripling the accumulation of N in protected SOM pools. Increases in  $V_{\max,\text{ref,mine}}$  and  $\tau_{\text{mine}}$  had the opposite effect, prolonging vegetation C accumulation through the end of the simulations and reducing protected N formation by over 50% (Figure S1).

### 3.2. Global Patterns of Plant N Acquisition and Soil N Cycling

Building upon the ecosystem-scale results, we performed global simulations to estimate the spatial distributions of different N acquisition strategies and their potential responses to rising atmospheric CO<sub>2</sub> levels. These simulations focused on natural ecosystems and did not include land use or agricultural fertilization.

Because soil N mineralization rates approached annual plant N requirements at steady state, soil inorganic N supplied the bulk of N requirements in most areas across the globe in control simulations, with a global annual mean uptake of 662.5 Tg N/year (Figure 4a). Inorganic N uptake (Figure 4a) was relatively higher in areas with higher atmospheric N deposition rates (Figure 6b). Global N uptake via mycorrhizal OM decomposition (Figure 4b) was substantially lower (205.9 Tg N/year). Although it was widely distributed, its relative contribution to total N acquisition was greatest in the boreal forest and tropics, areas with low inorganic N availability relative to vegetation N demand (Figures 4b and S2). While ECM-associated plants are commonly associated with high latitudes, there are significant observed populations of ECM-associated trees in tropical forests (Corrales et al., 2018). Modeled spatial distributions of AM and ECM fungi agreed with previous modeled estimates (Shi et al., 2016), and corresponded with observationally derived species distribution models (SDMs) with an 88% niche overlap for AM and 85.0% overlap for ECM. The high degree of overlap between model-derived and observation-derived SDMs suggests that our model accurately predicted these patterns. When converted to spatial maps (Figure 5), the model-based and observation-based distribution models both indicated higher likelihood of ECM presence in Scandinavia and higher likelihood of AM presence in most of Europe, China, and eastern North America. However, contrasts between AM and ECM spatial distributions were stronger in the observation-based SDM than in the model-based SDM.

Due to its higher relative cost, symbiotic N<sub>2</sub> fixation accounted for a smaller fraction of N uptake (46.1 Tg N/year; Figure 4c). Symbiotic N<sub>2</sub> fixation rates were within reported ranges of observation-based

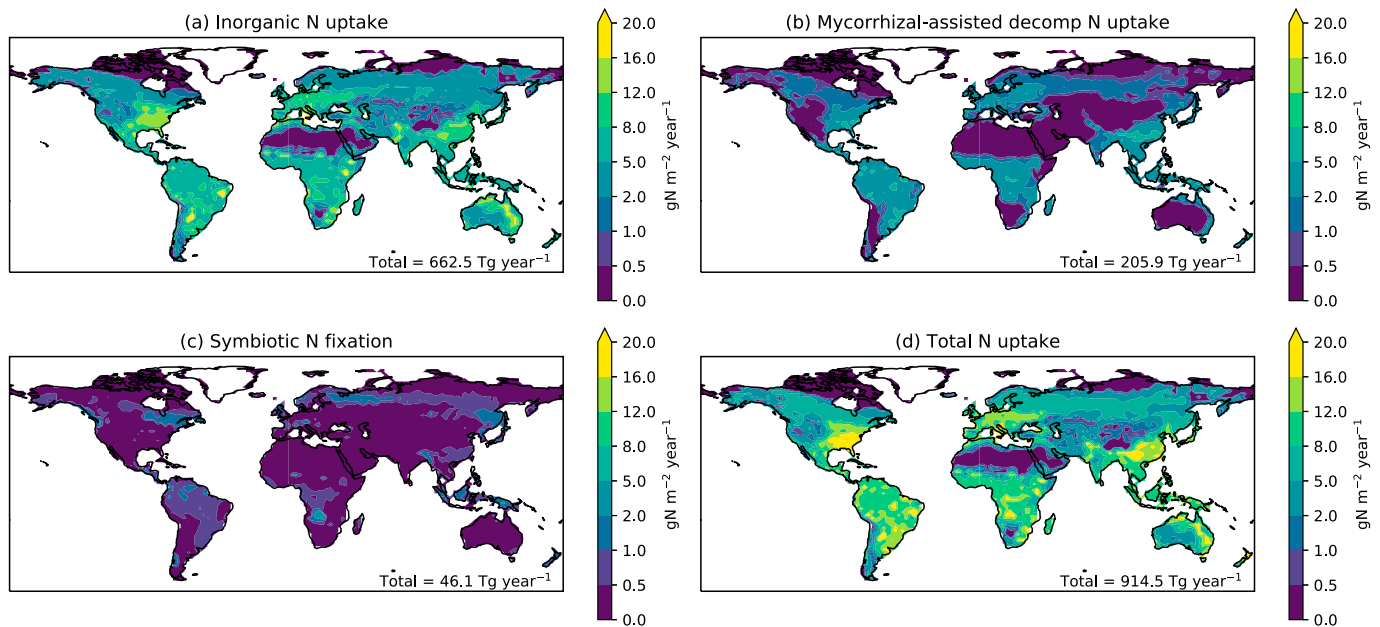


**Figure 4.** Global patterns of simulated N uptake at steady state. Note that the color scale is nonlinear. (a) Inorganic N uptake. (b) N uptake via mycorrhizal decomposition. (c) Symbiotic N<sub>2</sub> fixation. (d) Total N uptake.

estimates for the globe (less than 40 to over 100 Tg N/year; Cleveland et al., 1999; Vitousek et al., 2013) and for most biomes, except that the model-estimated N<sub>2</sub> fixation was higher in the boreal forest and lower in tundra than observation-based estimates (Table 1). Simulated N<sub>2</sub> fixation was near the mean observed value for tropical forest and on the lower side of the ranges of reported observations for deciduous forest and grassland.

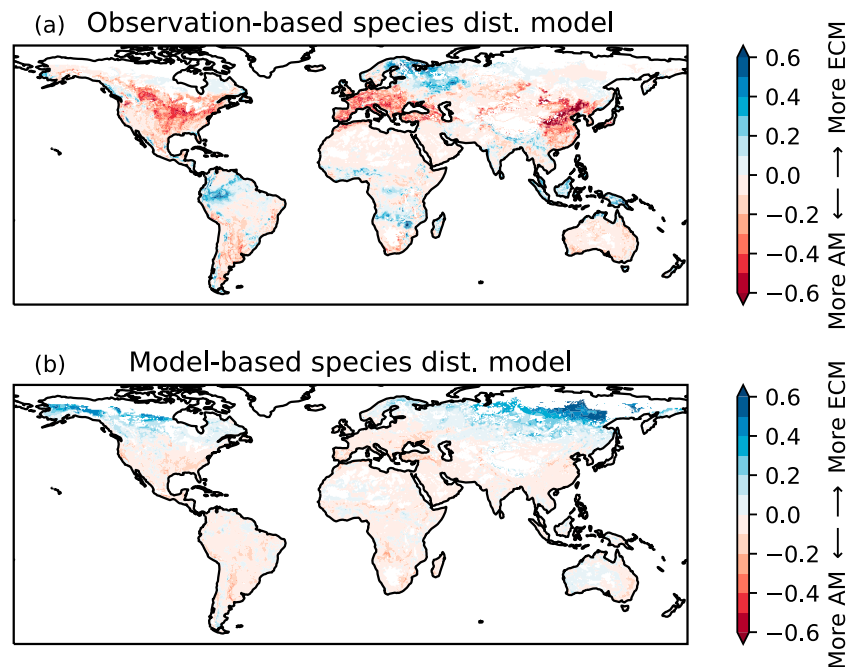


**Figure 5.** Differences between arbuscular mycorrhizal (AM) and Ectomycorrhiza (ECM) global distributions using species distribution models based on empirical data (see section 2.3) (a) and LM3-SNAP simulations (b). Species distribution models calculated a probability of presence in a grid cell between 0 and 1 for AM and ECM species. The maps show the AM distribution subtracted from the ECM distribution.

**Table 1**  
*Biome-Specific Symbiotic N Fixation Rates From Model and Literature*

Biome	Model values	Literature values
Boreal forest	5.2 (0.4, 12.4)	1.5–2.0 (0.3)
Deciduous forest	3.7 (1.3, 8.3)	6.5–26.6 (1.1–10.8)
Tropical forest	5.6 (1.9, 9.4)	5.7 (1.2–14)
Grassland	1.3 (0.0, 3.8)	2.3–3.1 (0.2–0.9)
Tundra	0.58 (0.0, 2.5)	2.8–9.4 (1.6–8.2)

*Note.* All values are in  $\text{kg N}\cdot\text{ha}^{-1}\cdot\text{year}^{-1}$ . Model values outside parentheses show the mean. Values in parentheses are 10th and 90th percentiles (on a grid cell basis). Literature values are estimated mean total N fixation from Cleveland et al. (1999) except for tropical forest, which uses Sullivan et al. (2014). Values in parentheses are reported ranges of observational estimates.

Differences in vegetation N acquisition strategies were associated with variations in soil N cycling. N mineralization was highest in temperate deciduous regions such as eastern North America and central Europe due to annual recycling of leaf litter and lowest in high latitudes (Figure 6a). These patterns were consistent with the higher contribution of inorganic N to plant uptake in temperate regions (Figure 4a). In addition, inputs of atmospheric N deposition were highest in temperate regions (Figure 6b), corresponding to areas with higher inorganic N uptake by plants. In higher latitudes where mycorrhizal-assisted decomposition was relatively more important, SOM was characterized by a higher C:N ratio (Figure 6c) and a higher unprotected fraction of soil N (Figure 6d). In tropical and temperate regions, SOM had a lower mean C:N ratio but the bulk of soil N stocks were trapped in protected pools.

### 3.3. Global Response to an Increase in CO<sub>2</sub>

To evaluate the role of symbiotic N acquisition in global-scale plant growth responses to rising atmospheric CO<sub>2</sub> levels, we simulated increased atmospheric CO<sub>2</sub> concentrations while holding climate forcing unchanged in a global manipulation that was analogous to the ecosystem-scale FACE experiments. We simulated three scenarios: One in which plant C allocations to different N acquisition symbioses changed dynamically in response to changing N demand (dynamic symbiotic allocations), one in which C allocations to symbioses were held constant but plant growth could be limited by N availability (static symbiotic allocations), and one in which plant growth was not N limited and symbiotic C allocations did not respond to changes in N availability or demand (no N limitation). Under a 100 ppm step increase in CO<sub>2</sub> concentration from 286 to 386 ppm, changes in plant symbiotic C allocations allowed C storage in vegetation biomass to increase by about 200 Pg C over 100 years (Figure 7d, blue lines). However, the increasing cost of N acquisition meant that enhancement of C uptake was lower than in a simulation with no N limitation (green lines).

In simulations with dynamic symbiotic allocations, inorganic N uptake increased by less than  $1 \text{ g N}\cdot\text{m}^{-2}\cdot\text{year}^{-1}$  in most regions, and declined in many areas as N immobilization increased (Figure 7e). Regions with substantial increases in inorganic N uptake coincided with higher rates of atmospheric N deposition and soil N mineralization (Figure 6b). The additional N demand from accelerated growth was largely met by a 100 Tg N/year increase in N uptake via mycorrhizal SOM decomposition and a 60 Tg N/year

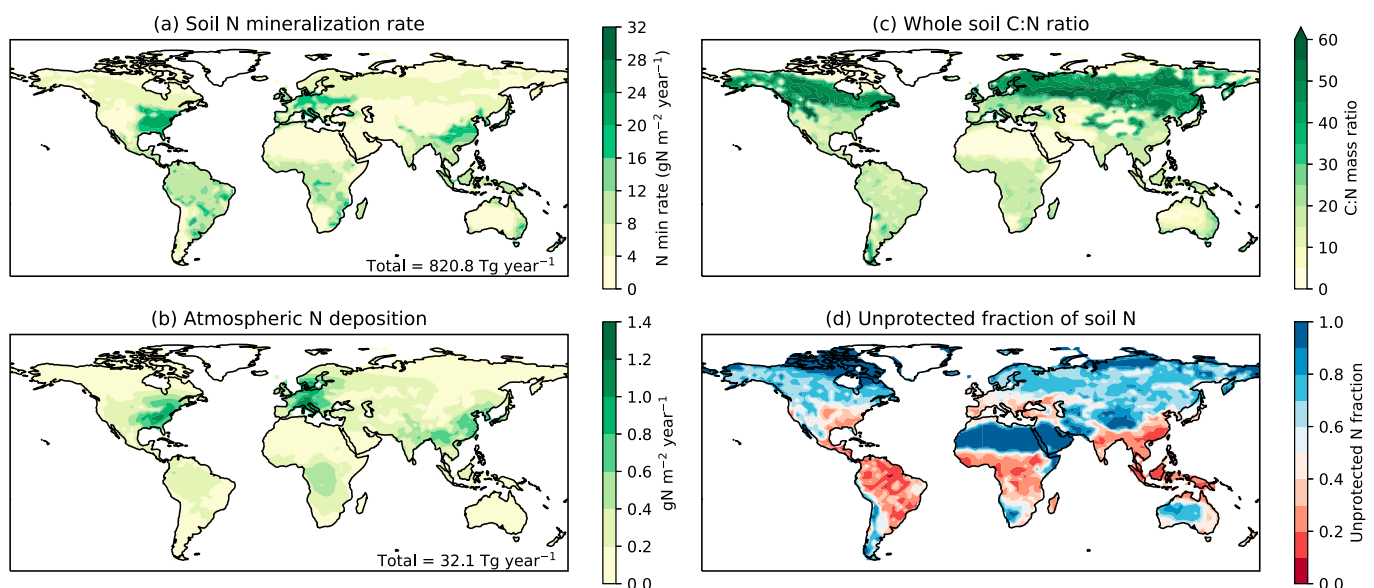


**Figure 6.** Modeled N cycle factors at global scales. (a) Total soil N mineralization rate. (b) Atmospheric N deposition flux. (c) Mean C:N ratio of the whole soil column (including organic horizons). (d): Fraction of soil N in unprotected pools.



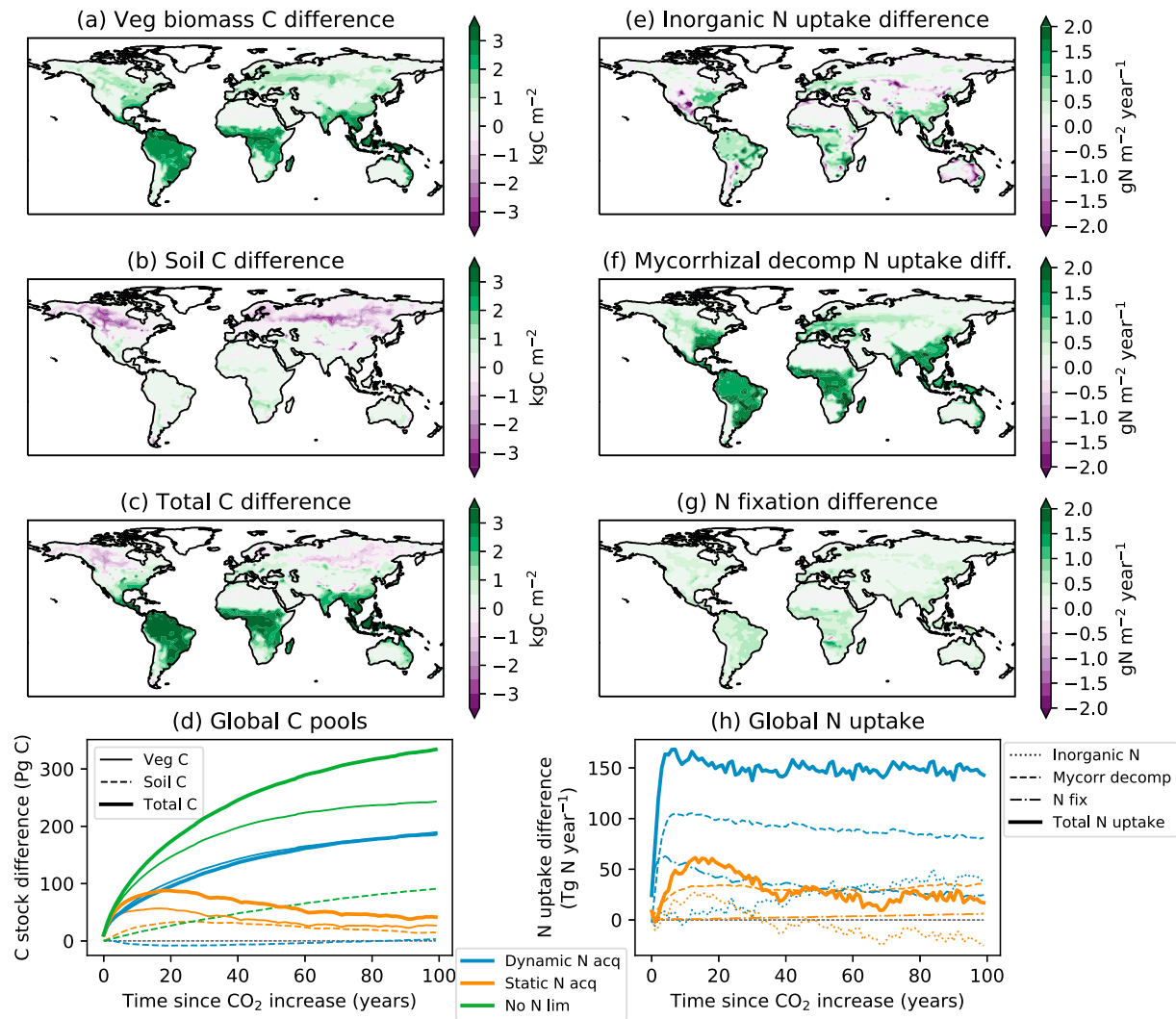


**Figure 7.** Modeled changes due to a 100-ppm increase in atmospheric CO<sub>2</sub> concentration. All plots show differences between elevated CO<sub>2</sub> and control simulations. (a–c) Differences in (a) vegetation, (b) soil, and (c) total C pools after 20 years, for simulations with dynamic symbiotic C allocations. (d) Globally integrated changes in C pools for simulations with dynamic symbiotic C allocations (blue), static symbiotic C allocations (orange), and no plant N limitation (green). (e–g): Changes in N acquisition via (e) inorganic N uptake, (f) SOM decomposition, and (g) N<sub>2</sub> fixation for simulations with dynamic symbiotic allocations. (h) Globally integrated changes in N acquisition rates. No N limitation simulations are shown because those simulations ignored N constraints.

increase in N<sub>2</sub> fixation (Figure 7h). Over time, increasing soil N stocks and mineralization rates allowed inorganic N uptake to gradually increase while N uptake from other sources declined. In contrast to our FACE site simulations, which did not include plants with N-fixing symbioses, enhanced vegetation growth in the global simulations was sustained for at least 100 years because trapping of N in protected SOM was counteracted by increases in N<sub>2</sub> fixation, which increased by about 1 g N·m<sup>-2</sup>·year<sup>-1</sup> in tropical and subtropical regions and by smaller amounts in higher latitudes (Figure 7g). Increases in N acquisition via mycorrhizal SOM decomposition were greatest (1.5–2 g N·m<sup>-2</sup>·year<sup>-1</sup>) in deciduous and tropical regions (Figure 7f). Smaller increases (0–1 g N·m<sup>-2</sup>·year<sup>-1</sup>) in the boreal forest reflected lower N requirements and greater longevity of roots and leaves.

Vegetation carbon gains with dynamic symbiotic allocations under elevated CO<sub>2</sub> were globally distributed, but highest in the tropics (Figure 7a). Enhanced mycorrhizal decomposition caused declines in soil C in some regions, particularly in high latitude regions with larger unprotected SOM stocks and higher C:N ratios (Figure 7b). This contributed to a slight decline in global soil C stocks over the first 60–70 years, after which the increased C inputs from growing vegetation caused global soil C stocks to increase again.

Simulations with static symbiotic allocations highlighted the importance of shifts in these N acquisition strategies for supporting accelerated growth. N uptake in these simulations was less responsive to elevated CO<sub>2</sub>, and inorganic N uptake was lower than control simulations following a transient 20-year increase at the beginning of the elevated CO<sub>2</sub> manipulation (Figure 7h, orange lines). While vegetation biomass initially increased by about 50 Pg C, it peaked after about 20 years and subsequently declined as N limitation worsened (Figure 7d, orange lines). Soil C stocks increased because there was limited mycorrhizal enhancement of SOM decomposition. However, total C accumulation under elevated CO<sub>2</sub> was substantially less than in simulations with dynamic symbiotic C allocations. In terms of land carbon sensitivity to CO<sub>2</sub> ( $\beta_L$ ; Friedlingstein et al., 2006), dynamic symbiotic allocations increased  $\beta_L$  by a factor of 4 relative to static symbiotic allocations, from 0.5 to 2 Pg C/ppm CO<sub>2</sub> after 100 years.

#### 4. Discussion and Conclusions

By incorporating fully coupled plant-mycorrhizal-soil interactions into a global-scale terrestrial C and N cycle model, LM3-SNAP represents a significant step forward in representing the extent to which coupled plant-microbial interactions influence whole ecosystem responses to changing environmental factors. Previous coupled global C-N cycle models have often treated vegetation and soil as somewhat disconnected sets of processes, with turnover of SOM pools proceeding at quasi-first-order rates independent from plant N demands (e.g., Gerber et al., 2010; Thomas et al., 2015; Zaehle, Friend, et al., 2010). Shi et al. (2016) implemented mycorrhizal C allocations in a global land model, but while that model simulated the C costs of N uptake it did not directly couple plant C acquisition to mycorrhizae with changes in soil C and N cycling. Our results demonstrate the importance of the fully coupled approach, showing how diversity in N acquisition strategies can allow ecosystems to maintain faster growth under elevated CO<sub>2</sub>.

The model successfully reproduced key observed patterns from the two ecosystem-scale experiments as well as global distributions of AM and ECM fungi. Measured protected soil C and N pools were higher at ORNL than at Duke, while unprotected and forest floor C and N were higher at Duke, and the model successfully reproduced these contrasts (Figure 2). Under elevated CO<sub>2</sub>, the model reproduced strong observed contrasts in plant growth and N uptake between the two sites (Figures 3a, 3c, 3e, and 3g) that have challenged models in previous comparisons (Zaehle et al., 2014). Differences in mycorrhizal N uptake strategies in the model could explain the strong growth response of the Duke experiment and the weak growth response of the ORNL experiment, supporting a hypothesis raised in a previous observational synthesis (Terrer et al., 2016). At global scales, species distribution models of ECM and AM fungal presence compared well between the model simulations and an independent, observation-based analysis, and rates of N fixation were consistent with observed patterns in most biomes (Table 1). Previous maps of mycorrhizal fungal distributions have been coarse (Allen et al., 1995), described continental-scale patterns only (Swaty et al., 2016), or lacked information on multiple mycorrhizal groups (e.g., Davison et al., 2015; Tedersoo et al., 2014). Thus, the observation-based maps represented here are a novel estimate of the spatial distributions of mycorrhizal fungal guilds. The high rates of modeled N<sub>2</sub> fixation in boreal forest suggest that the model may underestimate N availability in that biome, although there is evidence for significant N fixation in boreal forest moss layers (DeLuca et al., 2002).

The model simulations used in this study did omit some potentially important processes and reflected assumptions that may need further evaluation in the future. First, the model and analysis focused on N, and did not include other potentially important nutrients such as phosphorus (P). Recent studies have highlighted the role of P limitation in carbon cycle responses to elevated CO<sub>2</sub> at both ecosystem (Ellsworth et al., 2017) and global scales (Wieder et al., 2015). AM fungi play important roles in P acquisition (George et al., 1995), suggesting that patterns of symbiotic P acquisition could differ significantly from the patterns of N acquisition that were the focus of this manuscript. P limitation is likely to be particularly important in tropical regions (Peñuelas et al., 2013). Second, the model represented combinations of N uptake strategies as landscape-scale averages and did not directly simulate competitive interactions and reproductive processes that drive shifts in communities over time. We hope to combine the LM3-SNAP model with ongoing efforts to represent stand dynamics and interspecific competition in large-scale land models (Weng et al., 2017) in the future. Our simulations used step change increases in CO<sub>2</sub> rather than emulating historical and projected future patterns. This choice allowed us to draw parallels between ecosystem-scale and global

simulations and facilitated analysis of dynamical contrasts rather than historical patterns. However, the sudden changes in CO<sub>2</sub> concentration could have driven overestimates of N limitation compared to slower changes that would have allowed plant growth rates and soil N stocks to adjust more gradually. Further simulations using historical and projected rates of CO<sub>2</sub> accumulation are an important next step for this model framework. Finally, as with any complex ecosystem model parameterization of key processes remains a challenge. Important parameters such as mycorrhizal growth efficiencies and costs of N acquisition associated with different strategies could not be compared directly with measured quantities. While our model simulations compared well with ecosystem-scale measurements, the limitation of the ecosystem-scale validation to two sites with multiple contrasting traits (including mycorrhizal associations, leaf habits, and soil properties) leaves significant room for further model parameterization and validation. Our parameter sensitivity analysis indicated that results in ECM ecosystems were particularly sensitive to mycorrhizal N acquisition capacity and biomass turnover rates, which are currently challenging to constrain. This highlights the importance of continuing to develop measurement and model-data synthesis strategies that can further constrain these parameters. The much lower parameter sensitivity in the AM site suggested that ecosystem responses to elevated CO<sub>2</sub> in N limited, AM systems would be dominated by N availability rather than mycorrhizal N acquisition rates. We hope to further evaluate and constrain model parameters using more field experiments including both elevated CO<sub>2</sub> and N fertilization experiments in the future. Further model evaluation using global data sets of soil, vegetation, and N cycling would also be beneficial.

The coupling of the plant-mycorrhizal N acquisition model to a state-of-the-art SOM model incorporating microbial decomposition and mineral stabilization of SOM highlighted the importance of these mechanisms for driving key trends in N cycling over long time scales. Because protected SOM was primarily derived from microbial biomass (Bingham & Cotrufo, 2016; Cotrufo et al., 2013), it had a lower C:N ratio than either unprotected SOM or plant biomass. This meant that increasing accumulation of N in protected SOM pools drove a decline in ecosystem C storage. Thus, SNAP identifies an important mechanism by which physico-chemical SOM stabilization and symbiotic N acquisition interact to determine the ecosystem response to elevated CO<sub>2</sub>: The ability of ecosystems to delay N limitation and sustain terrestrial C uptake by decomposing SOM to extract N is ultimately limited by trapping of immobilized N in protected SOM. However, the timing of this effect was sensitive to rates of mycorrhizal-driven SOM decomposition.

Global simulations using our model highlighted a broad latitudinal variation in the bioavailable fraction of soil N. Soil N stocks were primarily protected via mineral associations in tropical and temperate regions, and were primarily unprotected in high-latitude regions. These contrasts resulted from three factors. First, leaf and root litter from evergreen needleleaf plants that dominate high latitudes had a higher initial C:N ratio than litter from temperate and tropical plant functional types, leading to a higher C:N ratio in organic matter that had not been microbially processed. Second, slower decomposition rates in high latitudes contributed to the accumulation of large unprotected SOM stocks with properties more similar to plant material, while rapid decomposition in tropical and temperate regions depleted unprotected SOM stocks and left most organic matter in protected pools that were primarily composed of microbially processed material with low C:N ratios close to that of microbial biomass. Third, tropical soils are likely to be highly weathered and often contain high concentrations of clays and reactive minerals (Jackson, 1959). The simulated patterns were consistent with observations showing that tropical soils contain relatively large stocks of mineral-associated organic matter and lower particulate SOM fractions (Bayer et al., 2002) while soils in higher latitudes often contain thick organic horizons and higher particulate SOM stocks (Hobbie et al., 2000). The structure of our model allows it to integrate a key consequence of these latitudinal contrasts for ecosystem responses to rising CO<sub>2</sub> levels: The higher unprotected fraction of high latitude SOM makes it particularly vulnerable to mycorrhizal decomposition as N becomes more limiting, leading to losses of SOC as plant growth increases. In tropical areas, there is less potential for SOC loss via these priming effects, but also a greater need for symbiotic N fixation to meet increased N demands.

The importance of multiple N acquisition pathways in our results highlights a potential weakness of global terrestrial C-N models that represent only plant uptake of inorganic N. Our results suggest that inorganic N has a limited capacity to support enhanced growth under elevated CO<sub>2</sub>. This is consistent with results from AM sites in a synthesis of elevated CO<sub>2</sub> experiments (Terrer et al., 2016) and with mechanisms included in previous ESM and DGVM studies indicating that inorganic N availability could limit the future terrestrial C

sink. For example, Thornton et al. (2009) found that inclusion of N limitation reduced  $\beta_L$  by a factor of three and Zaehle, Friedlingstein, et al. (2010) found that N limitation reduced terrestrial C uptake by a factor of two. These effects were slightly lower than the factor of four difference in  $\beta_L$  between dynamic and static symbiotic allocations in our global simulations. Our results suggest that ecosystem-level shifts toward mycorrhizal SOM decomposition and/or symbiotic N<sub>2</sub> fixation could mitigate such inorganic N limitation, making the capacity for such shifts a transformative factor in responses of terrestrial C uptake to elevated CO<sub>2</sub>.

The potential for long-term enhancement of terrestrial ecosystem C sequestration in N-limited systems thus hinges on a key question: To what extent can N acquisition strategies change at the ecosystem scale to satisfy increases in N demand? Plant species generally associate with a single mycorrhizal type (Lambers et al., 2008), and only a small subset of plant species can form N<sub>2</sub>-fixing symbioses (Huss-Danell, 1997; Sprent, 2009). Our results therefore suggest that an increase in global NPP under elevated CO<sub>2</sub> would require shifts in plant community composition toward species with ECM associations and/or N<sub>2</sub>-fixing symbioses. This suggests that functional diversity in plant communities plays an important role: C sequestration in ecosystems dominated by AM-associated species would likely be strongly N limited, while ecosystems including a mixture of AM, ECM and N<sub>2</sub>-fixing species could increase C uptake via shifts in relative growth toward species with more advantageous N acquisition symbioses. Temperate forests often encompass a diverse community of AM and ECM species (Fisher et al., 2016), suggesting that there is potential across large areas of the globe for shifts like the ones predicted by our model, although most N<sub>2</sub>-fixing tree species occur in tropical forests (Menge et al., 2017; ter Steege et al., 2006). While constraining key parameters controlling plant C allocations to symbioses and N acquisition rates of mycorrhizae remains a challenge, we believe that the important roles of alternate N acquisition strategies in our results support the value of incorporating these processes into models. Overall, incorporating diverse N acquisition symbioses and their ecosystem-scale plasticity into ESMs and DGVMs will improve representation of key terrestrial C and N cycle processes and could support more confident projections of the terrestrial C sink.

#### Acknowledgments

This report was prepared by B. Sulman under award NA14OAR4320106 from the National Oceanic and Atmospheric Administration, U.S. Department of Commerce. This study was also supported by NOAA Climate Program Office's Atmospheric Chemistry, Carbon Cycle, and Climate program, award NA15OAR4310065. The statements, findings, conclusions, and recommendations are those of the authors and do not necessarily reflect the views of the National Oceanic and Atmospheric Administration and the U.S. Department of Commerce. B. Sulman was also supported by the U.S. Department of Energy, Office of Biological and Environmental Research under contract number DE-AC05-00OR22725. E. Brzostek's contribution was supported by U.S. Department of Energy Office of Biological and Environmental Research, Terrestrial Ecosystem Science Program (award DESC0016188). X. Zhang's contribution was supported by Cooperative Institute for Climate Science, Princeton University under NOAA grant NA14OAR4320106. Thanks to Chiara Medici, Richard Phillips and Efrat Sheffer for helpful discussions. Data and code are posted on FigShare: doi:<https://doi.org/10.6084/m9.figshare.6207578>. These include ecosystem-scale simulation output, species distribution model data, global model output underlying all global plots, model code specific to the processes described in this manuscript, and analysis and plotting code. Full GFDL land model code is available upon request through the GFDL code management system.

#### References

- Allen, E. B., Allen, M. F., Helm, D. J., Trappe, J. M., Molina, R., & Rincon, E. (1995). Patterns and regulation of mycorrhizal plant and fungal diversity. *Plant and Soil*, *170*(1), 47–62. <https://doi.org/10.1007/BF02183054>
- Baskaran, P., Hyvönen, R., Berglund, S. L., Clemmensen, K. E., Ågren, G. I., Lindahl, B. D., & Manzoni, S. (2016). Modelling the influence of ectomycorrhizal decomposition on plant nutrition and soil carbon sequestration in boreal forest ecosystems. *New Phytologist*, *213*(3), 1452–1465. <https://doi.org/10.1111/nph.14213>
- Bayer, C., Mielniczuk, J., Martin-Neto, L., & Ernani, P. R. (2002). Stocks and humification degree of organic matter fractions as affected by no-tillage on a subtropical soil. *Plant and Soil*, *238*(1), 133–140. <https://doi.org/10.1023/A:1014284329618>
- Beedlow, P. A., Tingey, D. T., Phillips, D. L., Hogsett, W. E., & Olszyk, D. M. (2004). Rising atmospheric CO<sub>2</sub> and carbon sequestration in forests. *Frontiers in Ecology and the Environment*, *2*(6), 315–322. [https://doi.org/10.1890/1540-9295\(2004\)002\[0315:RACACS\]2.0.CO;2](https://doi.org/10.1890/1540-9295(2004)002[0315:RACACS]2.0.CO;2)
- Bingham, A. H., & Cotrufo, M. F. (2016). Organic nitrogen storage in mineral soil: Implications for policy and management. *Science of the Total Environment*, *551*–552, 116–126. <https://doi.org/10.1016/j.scitotenv.2016.02.020>
- Brzostek, E. R., Fisher, J. B., & Phillips, R. P. (2014). Modeling the carbon cost of plant nitrogen acquisition: Mycorrhizal trade-offs and multipath resistance uptake improve predictions of retranslocation. *Journal of Geophysical Research: Biogeosciences*, *119*, 1684–1697. <https://doi.org/10.1002/2014JG002660>
- Campbell, J. E., Berry, J. A., Seibt, U., Smith, S. J., Montzka, S. A., Launois, T., et al. (2017). Large historical growth in global terrestrial gross primary production. *Nature*, *544*(7648), 84–87. <https://doi.org/10.1038/nature22030>
- Cheng, W., Parton, W. J., Gonzalez-Meler, M. A., Phillips, R., Asao, S., McNickle, G. G., et al. (2014). Synthesis and modeling perspectives of rhizosphere priming. *New Phytologist*, *201*(1), 31–44. <https://doi.org/10.1111/nph.12440>
- Ciais, P., Sabine, C., Bala, G., Bopp, L., Brovkin, V., Canadell, J., et al. (2013). Carbon and other biogeochemical cycles. In T. F. Stocker, D. Qin, G.-K. Plattner, M. Tignor, S. K. Allen, J. Boschung, A. Nauels, Y. Xia, V. Bex, & P. M. Midgley (Eds.), *Climate change 2013: The physical science basis. Contribution of Working Group I to the Fifth Assessment Report of the Intergovernmental Panel on Climate Change* (pp. 465–570). Cambridge, UK and New York: Cambridge University Press.
- Cleveland, C. C., Townsend, A. R., Schimel, D. S., Fisher, H., Howarth, R. W., Hedin, L. O., et al. (1999). Global patterns of terrestrial biological nitrogen (N<sub>2</sub>) fixation in natural ecosystems. *Global Biogeochemical Cycles*, *13*(2), 623–645. <https://doi.org/10.1029/1999GB900014>
- Cole, C. T., Anderson, J. E., Lindroth, R. L., & Waller, D. M. (2009). Rising concentrations of atmospheric CO<sub>2</sub> have increased growth in natural stands of quaking aspen (*Populus tremuloides*). *Global Change Biology*, *16*(8), 2186–2197. <https://doi.org/10.1111/j.1365-2486.2009.02103.x>
- Corrales, A., Henkel, T. W., & Smith, M. E. (2018). Ectomycorrhizal associations in the tropics – biogeography, diversity patterns and ecosystem roles. *New Phytologist*, *220*(4), 1076–1091. <https://doi.org/10.1111/nph.15151>
- Cotrufo, M. F., Wallenstein, M. D., Boot, C. M., Deneff, K., & Paul, E. A. (2013). The Microbial Efficiency-Matrix Stabilization (MEMS) framework integrates plant litter decomposition with soil organic matter stabilization: Do labile plant inputs form stable soil organic matter? *Global Change Biology*, *19*, 988–995. <https://doi.org/10.1111/gcb.12113>

- Davison, J., Moora, M., Opik, M., Adholeya, A., Ainsaar, L., Ba, A., et al. (2015). Global assessment of arbuscular mycorrhizal fungus diversity reveals very low endemism. *Science*, *349*(6251), 970–973. <https://doi.org/10.1126/science.aab1161>
- DeLuca, T. H., Zackrisson, O., Nilsson, M.-C., & Sellstedt, A. (2002). Quantifying nitrogen-fixation in feather moss carpets of boreal forests. *Nature*, *419*(6910), 917–920. <https://doi.org/10.1038/nature01051>
- Drake, J. E., Gallet-Budynek, A., Hofmockel, K. S., Bernhardt, E. S., Billings, S. A., Jackson, R. B., et al. (2011). Increases in the flux of carbon belowground stimulate nitrogen uptake and sustain the long-term enhancement of forest productivity under elevated CO<sub>2</sub>. *Ecology Letters*, *14*(4), 349–357.
- Ellsworth, D. S., Anderson, I. C., Crous, K. Y., Cooke, J., Drake, J. E., Gherlenda, A. N., et al. (2017). Elevated CO<sub>2</sub> does not increase eucalypt forest productivity on a low-phosphorus soil. *Nature Climate Change*, *7*(4), 279–282. <https://doi.org/10.1038/nclimate3235>
- Finzi, A. C., Abramoff, R. Z., Spiller, K. S., Brzostek, E. R., Darby, B. A., Kramer, M. A., & Phillips, R. P. (2015). Rhizosphere processes are quantitatively important components of terrestrial carbon and nutrient cycles. *Global Change Biology*, *21*(5), 2082–2094. <https://doi.org/10.1111/gcb.12816>
- Finzi, A. C., Allen, A. S., DeLucia, E. H., Ellsworth, D. S., & Schlesinger, W. H. (2001). Forest litter production, chemistry, and decomposition following two years of free-air CO<sub>2</sub> enrichment. *Ecology*, *82*(2), 470–484. [https://doi.org/10.1890/0012-9658\(2001\)082\[0470:FLPCAD\]2.0.CO;2](https://doi.org/10.1890/0012-9658(2001)082[0470:FLPCAD]2.0.CO;2)
- Finzi, A. C., Norby, R. J., Calfapietra, C., Gallet-Budynek, A., Gielen, B., Holmes, W. E., et al. (2007). Increases in nitrogen uptake rather than nitrogen-use efficiency support higher rates of temperate forest productivity under elevated CO<sub>2</sub>. *Proceedings of the National Academy of Sciences of the United States of America*, *104*(35), 14,014–14,019. <https://doi.org/10.1073/pnas.0706518104>
- Fisher, J. B., Sweeney, S., Brzostek, E. R., Evans, T. P., Johnson, D. J., Myers, J. A., et al. (2016). Tree-mycorrhizal associations detected remotely from canopy spectral properties. *Global Change Biology*, *22*(7), 2596–2607. <https://doi.org/10.1111/gcb.13264>
- Friedlingstein, P., Cox, P., Betts, R., Bopp, L., von Bloh, W., Brovkin, V., et al. (2006). Climate-carbon cycle feedback analysis: Results from the C4MIP model Intercomparison. *Journal of Climate*, *19*(14), 3337–3353. <https://doi.org/10.1175/JCLI3800.1>
- George, E., Marschner, H., & Jakobsen, I. (1995). Role of arbuscular mycorrhizal fungi in uptake of phosphorus and nitrogen from soil. *Critical Reviews in Biotechnology*, *15*(3–4), 257–270. <https://doi.org/10.3109/07388559509147412>
- Gerber, S., Hedin, L. O., Oppenheimer, M., Pacala, S. W., & Shevliakova, E. (2010). Nitrogen cycling and feedbacks in a global dynamic land model. *Global Biogeochemical Cycles*, *24*, GB1001. <https://doi.org/10.1029/2008GB003336>
- Green, P. A., Vorosmarty, C. J., Meybeck, M., Galloway, J. N., Peterson, B. J., & Boyer, E. W. (2004). Pre-industrial and contemporary fluxes of nitrogen through rivers: a global assessment based on typology. *Biogeochemistry*, *68*(1), 71–105. <https://doi.org/10.1023/B:BIOG.0000025742.82155.92>
- Heinen, M. (2006). Application of a widely used denitrification model to Dutch data sets. *Geoderma*, *133*(3–4), 464–473. <https://doi.org/10.1016/j.geoderma.2005.08.011>
- Hobbie, S. E., Schimel, J. P., Trumbore, S. E., & Randerson, J. R. (2000). Controls over carbon storage and turnover in high-latitude soils. *Global Change Biology*, *6*(S1), 196–210. <https://doi.org/10.1046/j.1365-2486.2000.06021.x>
- Houlton, B. Z., Wang, Y.-P., Vitousek, P. M., & Field, C. B. (2008). A unifying framework for dinitrogen fixation in the terrestrial biosphere. *Nature*, *454*(7202), 327–330. <https://doi.org/10.1038/nature07028>
- Hungate, B. A., Dukes, J. S., Shaw, M. R., Luo, Y., & Field, C. B. (2003). Nitrogen and climate change. *Science*, *302*, 1512.
- Huss-Danell, K. (1997). Actinorhizal symbioses and their N<sub>2</sub> fixation. *New Phytologist*, *136*(3), 375–405. <https://doi.org/10.1046/j.1469-8137.1997.00755.x>
- Iversen, C. M., Keller, J. K., Garten, C. T. Jr., & Norby, R. J. (2012). Soil carbon and nitrogen cycling and storage throughout the soil profile in a sweetgum plantation after 11 years of CO<sub>2</sub>-enrichment. *Global Change Biology*, *18*(5), 1684–1697. <https://doi.org/10.1111/j.1365-2486.2012.02643.x>
- Jackson, M. L. (1959). Frequency distribution of clay minerals in major great soil groups as related to the factors of soil formation. *Clays and Clay Minerals*, *6*, 133–143.
- Jastrow, J. D., Michael Miller, R., Matamala, R., Norby, R. J., Boutton, T. W., Rice, C. W., & Owensby, C. E. (2005). Elevated atmospheric carbon dioxide increases soil carbon. *Global Change Biology*, *11*(12), 2057–2064. <https://doi.org/10.1111/j.1365-2486.2005.01077.x>
- Keenan, T. F., Prentice, I. C., Canadell, J. G., Williams, C. A., Wang, H., Raupach, M., & Collatz, G. J. (2016). Recent pause in the growth rate of atmospheric CO<sub>2</sub> due to enhanced terrestrial carbon uptake. *Nature Communications*, *7*(1), 13428. <https://doi.org/10.1038/ncomms13428>
- Kivlin, S. N., Emery, S. M., & Rudgers, J. A. (2013). Fungal symbionts alter plant responses to global change. *American Journal of Botany*, *100*(7), 1445–1457. <https://doi.org/10.3732/ajb.1200558>
- Kivlin, S. N., Muscarella, R., Hawkes, C. V., & Treseder, K. K. (2017). The predictive power of ecological niche modeling for global arbuscular mycorrhizal fungal biogeography. In *Biogeography of Mycorrhizal Symbiosis* (Vol. 230, pp. 143–158). Cham: Springer.
- Körner, C. (2006). Plant CO<sub>2</sub> responses: an issue of definition, time and resource supply. *New Phytologist*, *172*(3), 393–411. <https://doi.org/10.1111/j.1469-8137.2006.01886.x>
- Lambers, H., Raven, J., Shaver, G., & Smith, S. (2008). Plant nutrient-acquisition strategies change with soil age. *Trends in Ecology & Evolution*, *23*(2), 95–103. <https://doi.org/10.1016/j.tree.2007.10.008>
- Le Quere, C., Andrew, R. M., Friedlingstein, P., Sitch, S., Hauck, J., Pongratz, J., et al. (2018). Global carbon budget 2018. *Earth System Science Data*, *10*, 2141–2194. <https://doi.org/10.5194/essd-10-2141-2018>
- Lichter, J., Barron, S. H., Bevacqua, C. E., Finzi, A. C., Irving, K. F., Stemmler, E. A., & Schlesinger, W. H. (2005). Soil carbon sequestration and turnover in a pine forest after six years of atmospheric CO<sub>2</sub> enrichment. *Ecology*, *86*(7), 1835–1847. <https://doi.org/10.1890/04-1205>
- Lichter, J., Billings, S. A., Ziegler, S. E., Gaidh, D., Ryals, R., Finzi, A. C., et al. (2008). Soil carbon sequestration in a pine forest after 9 years of atmospheric CO<sub>2</sub> enrichment. *Global Change Biology*, *14*(12), 2910–2922. <https://doi.org/10.1111/j.1365-2486.2008.01701.x>
- Menge, D. N. L., Batterman, S. A., Liao, W., Taylor, B. N., Lichstein, J. W., & Ángeles Pérez, G. (2017). Nitrogen-fixing tree abundance in higher-latitude North America is not constrained by diversity. *Ecology Letters*, *20*(7), 842–851. <https://doi.org/10.1111/ele.12778>
- Millard, P., Hester, A., Wendler, R., & Baillie, G. (2001). Interspecific defoliation responses of trees depend on sites of winter nitrogen storage. *Functional Ecology*, *15*(4), 535–543. <https://doi.org/10.1046/j.0269-8463.2001.00541.x>
- Milly, P. C. D., Malyshev, S. L., Shevliakova, E., Dunne, K. A., Findell, K. L., Gleeson, T., et al. (2014). An enhanced model of land water and energy for global hydrologic and earth-system studies. *Journal of Hydrometeorology*, *15*, 1739–1761. <https://doi.org/10.1175/JHM-D-13-0162.1>

- Muscarella, R., Galante, P. J., Soley-Guardia, M., Boria, R. A., Kass, J. M., Uriarte, M., & Anderson, R. P. (2014). ENMeval: An R package for conducting spatially independent evaluations and estimating optimal model complexity for Maxent ecological niche models. *Methods in Ecology and Evolution*, 5(11), 1198–1205. <https://doi.org/10.1111/2041-210X.12261>
- Norby, R. J., De Kauwe, M. G., Walker, A. P., Werner, C., Zaehle, S., & Zak, D. R. (2017). Comment on “Mycorrhizal association as a primary control of the CO<sub>2</sub> fertilization effect”. *Science*, 355(6232), 358–358. <https://doi.org/10.1126/science.aai7976>
- Norby, R. J., Hanson, P. J., O'Neill, E. G., Tschaplinski, T. J., Weltzin, J. F., Hansen, R. A., et al. (2002). Net primary productivity of a CO<sub>2</sub>-enriched deciduous forest and the implications for carbon storage. *Ecological Applications*, 12(5), 1261–1266.
- Norby, R. J., Oren, R., Boden, T. A., De Kauwe, M. G., Kim, D., Medlyn, B. E., et al. (2015). Phase 1 Free Air CO<sub>2</sub> Enrichment Model-Data Synthesis (FACE-MDS): Meteorological data. <https://doi.org/10.3334/CDIAC/FACE-MDS/MET.01>
- Norby, R. J., Warren, J. M., Iversen, C. M., Medlyn, B. E., & McMurtrie, R. E. (2010). CO<sub>2</sub> enhancement of forest productivity constrained by limited nitrogen availability. *Proceedings of the National Academy of Sciences of the United States of America*, 107(45), 19,368–19,373.
- Norby, R. J., & Zak, D. R. (2011). Ecological lessons from Free-Air CO<sub>2</sub> Enrichment (FACE) Experiments. *Annual Review of Ecology, Evolution, and Systematics*, 42(1), 181–203. <https://doi.org/10.1146/annurev-ecolsys-102209-144647>
- Öpik, M., Vanatoa, A., Vanatoa, E., Moora, M., Davison, J., Kalwij, J. M., et al. (2010). The online database MaarjAM reveals global and ecosystemic distribution patterns in arbuscular mycorrhizal fungi (Glomeromycota). *New Phytologist*, 188(1), 223–241. <https://doi.org/10.1111/j.1469-8137.2010.03334.x>
- Orwin, K. H., Kirschbaum, M. U. F., St John, M. G., & Dickie, I. A. (2011). Organic nutrient uptake by mycorrhizal fungi enhances ecosystem carbon storage: A model-based assessment. *Ecology Letters*, 14(5), 493–502. <https://doi.org/10.1111/j.1461-0248.2011.01611.x>
- Pellitier, P. T., & Zak, D. R. (2017). Ectomycorrhizal fungi and the enzymatic liberation of nitrogen from soil organic matter: Why evolutionary history matters. *New Phytologist*, 103, 495–496. <https://doi.org/10.1111/nph.14598>
- Peñuelas, J., Poulter, B., Sardans, J., Ciais, P., van der Velde, M., Bopp, L., et al. (2013). Human-induced nitrogen–phosphorus imbalances alter natural and managed ecosystems across the globe. *Nature Communications*, 4(1), 2934. <https://doi.org/10.1038/ncomms3934>
- Phillips, R. P., Bernhardt, E. S., & Schlesinger, W. H. (2009). Elevated CO<sub>2</sub> increases root exudation from loblolly pine (*Pinus taeda*) seedlings as an N-mediated response. *Tree Physiology*, 29(12), 1513–1523.
- Phillips, R. P., Meier, I. C., Bernhardt, E. S., Grandy, A. S., Wickings, K., & Finzi, A. C. (2012). Roots and fungi accelerate carbon and nitrogen cycling in forests exposed to elevated CO<sub>2</sub>. *Ecology Letters*, 15, 1042–1049.
- Phillips, S. J., Anderson, R. P., & Schapire, R. E. (2006). Maximum entropy modeling of species geographical distributions. *Ecological Modelling*, 190, 231–259.
- Read, D. J., & Perez Moreno, J. (2003). Mycorrhizas and nutrient cycling in ecosystems—A journey towards relevance? *New Phytologist*, 157(3), 475–492. <https://doi.org/10.1046/j.1469-8137.2003.00704.x>
- Schlesinger, W. H., Bernhardt, E. S., DeLucia, E. H., Ellsworth, D. S., Finzi, A. C., Hendrey, G. R., et al. (2006). The Duke forest FACE experiment: CO<sub>2</sub> enrichment of a loblolly pine forest. In M. M. Caldwell, G. Heldmaier, R. B. Jackson, O. L. Lange, H. A. Mooney, E. D. Schulze, & U. Sommer (Eds.), *Managed Ecosystems and CO<sub>2</sub>* (Vol. 187, pp. 197–212). Berlin/Heidelberg: Springer. [https://doi.org/10.1007/3-540-31237-4\\_11](https://doi.org/10.1007/3-540-31237-4_11)
- Schmidt, M. W. I., Torn, M. S., Abiven, S., Dittmar, T., Guggenberger, G., Janssens, I. A., et al. (2011). Persistence of soil organic matter as an ecosystem property. *Nature*, 478(7367), 49–56. <https://doi.org/10.1038/nature10386>
- Sheffield, J., Goteti, G., & Wood, E. F. (2006). Development of a 50-year high-resolution global dataset of meteorological forcings for land surface modeling. *Journal of Climate*, 19(13), 3088–3111. <https://doi.org/10.1175/JCLI3790.1>
- Shevliakova, E., Pacala, S. W., Malyshev, S., Hurtt, G. C., Milly, P. C. D., Caspersen, J. P., et al. (2009). Carbon cycling under 300 years of land use change: Importance of the secondary vegetation sink. *Global Biogeochemical Cycles*, 23, GB2022. <https://doi.org/10.1029/2007GB003176>
- Shi, M., Fisher, J. B., Brzostek, E. R., & Phillips, R. P. (2016). Carbon cost of plant nitrogen acquisition: global carbon cycle impact from an improved plant nitrogen cycle in the Community Land Model. *Global Change Biology*, 22(3), 1299–1314. <https://doi.org/10.1111/gcb.13131>
- Sprent, J. I. (2009). Legume nodulation: A global perspective. <https://doi.org/10.1002/9781444316384>
- Sullivan, B. W., Smith, W. K., Townsend, A. R., Nasto, M. K., Reed, S. C., Chazdon, R. L., & Cleveland, C. C. (2014). Spatially robust estimates of biological nitrogen (N) fixation imply substantial human alteration of the tropical N cycle. *Proceedings of the National Academy of Sciences of the United States of America*, 111(22), 8101–8106. <https://doi.org/10.1073/pnas.1320646111>
- Sulman, B. N., Brzostek, E. R., Medici, C., Shevliakova, E., Menge, D. N. L., & Phillips, R. P. (2017). Feedbacks between plant N demand and rhizosphere priming depend on type of mycorrhizal association. *Ecology Letters*, 20, 1043–1053. <https://doi.org/10.1111/ele.12802>
- Sulman, B. N., Phillips, R. P., Oishi, A. C., Shevliakova, E., & Pacala, S. W. (2014). Microbe-driven turnover offsets mineral-mediated storage of soil carbon under elevated CO<sub>2</sub>. *Nature Climate Change*, 4, 1099–1102. <https://doi.org/10.1038/nclimate2436>
- Swaty, R., Michael, H. M., Deckert, R., & Gehring, C. A. (2016). Mapping the potential mycorrhizal associations of the conterminous United States of America. *Fungal Ecology*, 24, 139–147. <https://doi.org/10.1016/j.funeco.2016.05.005>
- Tedersoo, L., Bahram, M., Pölme, S., Kõljalg, U., Yorou, N. S., Wijesundera, R., et al. (2014). Fungal biogeography: Global diversity and geography of soil fungi. *Science*, 346(6213), 1256688. <https://doi.org/10.1126/science.1256688>
- ter Steege, H., Pitman, N. C., Phillips, O. L., Chave, J., D., Duque, A., et al. (2006). Continental-scale patterns of canopy tree composition and function across Amazonia. *Nature*, 443(7110), 444–447. <https://doi.org/10.1038/nature05134>
- Terrer, C., Vicca, S., Hungate, B. A., Phillips, R. P., & Prentice, I. C. (2016). Mycorrhizal association as a primary control of the CO<sub>2</sub> fertilization effect. *Science*, 353(6294), 72–74. <https://doi.org/10.1126/science.aaf4610>
- Terrer, C., Vicca, S., Stocker, B. D., Hungate, B. A., Phillips, R. P., Reich, P. B., et al. (2017). Ecosystem responses to elevated CO<sub>2</sub> governed by plant–soil interactions and the cost of nitrogen acquisition. *New Phytologist*, 217(2), 507–522. <https://doi.org/10.1111/nph.14872>
- Thomas, R. Q., Brookshire, E. N. J., & Gerber, S. (2015). Nitrogen limitation on land: How can it occur in Earth system models? *Global Change Biology*, 21(5), 1777–1793. <https://doi.org/10.1111/gcb.12813>
- Thornton, P., Doney, S., Lindsay, K., Moore, J., Mahowald, N., Randerson, J., et al. (2009). Carbon-nitrogen interactions regulate climate-carbon cycle feedbacks: Results from an atmosphere-ocean general circulation model. *Biogeosciences*, 6, 2099–2120.
- Thornton, P. E., Lamarque, J. F., Rosenbloom, N. A., & Mahowald, N. M. (2007). Influence of carbon-nitrogen cycle coupling on land model response to CO<sub>2</sub> fertilization and climate variability. *Global Biogeochemical Cycles*, 21, GB4018. <https://doi.org/10.1029/2006GB002868>
- Vitousek, P. M., Menge, D. N. L., Reed, S. C., & Cleveland, C. C. (2013). Biological nitrogen fixation: rates, patterns and ecological controls in terrestrial ecosystems. *Philosophical Transactions of the Royal Society of London. Series B, Biological Sciences*, 368(1621), 20130119. <https://doi.org/10.1098/rstb.2013.0119>

- Warren, D. L., Glor, R. E., & Turelli, M. (2008). Environmental niche equivalency versus conservatism: Quantitative approaches to niche evolution. *Evolution*, *62*(11), 2868–2883. <https://doi.org/10.1111/j.1558-5646.2008.00482.x>
- Warren, J. M., Pötzelsberger, E., Wullschleger, S. D., Thornton, P. E., Hasenauer, H., & Norby, R. J. (2011). Ecohydrologic impact of reduced stomatal conductance in forests exposed to elevated CO<sub>2</sub>. *Ecohydrology*, *4*(2), 196–210. <https://doi.org/10.1002/eco.173>
- Weng, E., Farrior, C. E., Dybzinski, R., & Pacala, S. W. (2017). Predicting vegetation type through physiological and environmental interactions with leaf traits: Evergreen and deciduous forests in an earth system modeling framework. *Global Change Biology*, *23*(6), 2482–2498. <https://doi.org/10.1111/gcb.13542>
- Wieder, W. R., Cleveland, C. C., Smith, W. K., & Todd-Brown, K. (2015). Future productivity and carbon storage limited by terrestrial nutrient availability. *Nature Geoscience*, *8*(6), 441–444. <https://doi.org/10.1038/ngeo2413>
- Yuan, Y., Zhao, W., Zhang, Z., Xiao, J., Li, D., Liu, Q., & Yin, H. (2018). Impacts of oxalic acid and glucose additions on N transformation in microcosms via artificial roots. *Soil Biology and Biochemistry*, *121*, 16–23. <https://doi.org/10.1016/j.soilbio.2018.03.002>
- Zaehle, S., Friedlingstein, P., & Friend, A. D. (2010). Terrestrial nitrogen feedbacks may accelerate future climate change. *Geophysical Research Letters*, *37*, L01401. <https://doi.org/10.1029/2009GL041345>
- Zaehle, S., Friend, A. D., Friedlingstein, P., Dentener, F., Peylin, P., & Schulz, M. (2010). Carbon and nitrogen cycle dynamics in the O-CN land surface model: 2. Role of the nitrogen cycle in the historical terrestrial carbon balance. *Global Biogeochemical Cycles*, *24*, GB1006. <https://doi.org/10.1029/2009GB003522>
- Zaehle, S., Medlyn, B. E., de Kauwe, M. G., Walker, A. P., Dietze, M. C., Hickler, T., et al. (2014). Evaluation of 11 terrestrial carbon-nitrogen cycle models against observations from two temperate free-air CO<sub>2</sub> enrichment studies. *New Phytologist*, *202*(3), 803–822. <https://doi.org/10.1111/nph.12697>
- Zhang, Q., Wang, Y.-P., Mearns, R. J., Pitman, A. J., & Dai, Y. J. (2014). Nitrogen and phosphorous limitations significantly reduce future allowable CO<sub>2</sub> emissions. *Geophysical Research Letters*, *41*, 632–637. <https://doi.org/10.1002/2013GL058352>